CHAPTER
2 Instrumentation

Robert C. Dunbar and Bruce Asamoto

Introduction

FT-ICR MS instrumentation is still in a state of rapid development. The previous chapter traced the evolution of the technique up through the mid-1980s. At that point, when a few dozen instruments were in use, FT-ICR MS had already established its ability to give routinely higher mass accuracy and higher mass resolution than most magnetic sector (and all quadrupole) instruments.

In this chapter, we will review some standard methods of ionization, excitation, and detection. Hardware aspects of ICR cell design, magnets, and overall instrument configurations will be described to provide some insight into what is or may become commercially available. Another section will discuss performance characteristics for FT-ICR MS and compare these parameters with traditional types of mass analyzers. In some cases we will defer to a more thorough discussion of a topic in one of the later chapters (e.g., suspended trapping in Chapter 3 and mass accuracy in Chapter 9).

There will be some emphasis on three areas of rapid progress in the current development of the technique. Progress in the area of understanding ion motions gives the hope of cell designs that will further improve the resolution, mass accuracy, and peak quantitation capabilities. In the area of excitation and detection, tailored excitation and other advanced excitation and signal-processing techniques are greatly improving flexibility, dynamic range, quantitation, and MS/MS capabilities. Lastly, the development of more effective, varied, and versatile ion-production methods, especially the use of ionization sources external to the magnet, is improving the compatibility of FT-ICR MS with conventional ion sources.

Ionization and Ion Activation

Ionization for FT-ICR MS can be classified as either occurring within the homogeneous high magnetic field region or external to the magnetic field. Because of difficulties in moving ions from the weak- to strong-field region, early designs focused on ionization within the magnet. Most of the common MS ionization techniques have now been demonstrated within the magnet with varying degrees of success. Although this removes the problem of ion transfer, sample introduction or the ionization technique itself may impose a high gas load on the system that is detrimental to high-resolution detection. Developments such as the EXTREL dual cell are simple in concept and allow differential pumping to accomodate certain of these sample introduction and ionization techniques. An alternative is provided by external ion source instruments. Not only does this design overcome obstacles associated with designing an ion source to operate in the magnet bore, but it also makes available to FT-ICR MS the wealth of source hardware that has been designed for conventional mass spectrometers. A consensus on the "best" design does not exist, and factors such as cost, simplicity of design and operation, and primary applications must be considered. Both dual-cell and external ion source instruments are well represented in this book.

Ionization Within the Magnetic Field

The evolution of ion sources and ionization techniques based on producing the ions within the high-field region has been governed by several features of the FT-ICR instrument:

The geometry is constrained, so that the source must be specially designed to fit within or aligned along the magnet bore. It is difficult to adapt those source technologies such as supersonic beam expansion, thermospray, and electrospray, which require rapid, local differential pumping to deal with large gas loads.

The analyzer must achieve very good vacuum ($\sim 10^{-8}$ torr) to take advantage of the instrument's mass resolution potential. Therefore, differentially pumped source technologies have to be enormously efficient.

The analyzer is intolerant of strong electric fields. The high-field techniques of field desorption and field ionization have been slow to be adapted, because it is not easy to shield the ICR analyzer from the high source electric fields and to control the high ion velocities associated with these fields.

The ICR trap stores ions. It is thus particularly well suited to ^{252}Cf ionization, where ions are produced singly at random times and can profitably be accumulated in the trap, and to pulsed-laser tech-

niques including laser desorption (LD)-ionization, multiphoton ionization (MPI), and LD with subsequent EI or CI ionization, where a single large burst of ions is produced at essentially the same time.

The analyzer is tolerant of velocity and space dispersion. Ionization techniques such as LD, which spray ions out with a wide velocity distribution and poorly defined geometry, can be efficiently used because the ICR cell can trap a large percentage of these ions.

Electron Ionization

Electron ionization (EI) presents no special problems within a magnetic field. There is some difficulty with a filament in a high-field region because of the force on the filament from the electron current flow interacting with the magnetic field. However, in the superconducting magnet geometry, the magnetic field acts to collimate the electron beam as it passes through the ICR cell. Electrons can be efficiently introduced into the cell from a filament that is located in a region where the magnetic field is many times weaker than in the central bore.

Chemical Ionization

Chemical ionization (CI) can be easily implemented with no additional hardware (1). In standard CI, high reagent gas pressures are used to optimize the reagent ion and product ion formation. By contrast, in FT-ICR MS a low pressure of reagent gas is used, and a delay of tens to hundreds of milliseconds is provided between the electron beam pulse and the ICR detection event. This gives the initially produced reagent ions time for the large number of collisions with neutral molecules needed for CI to occur, while maintaining the low cell pressure needed for optimal ion detection. Self-CI, where the initial EI-produced ions constitute the CI reagent species, is also easily performed. The use of pulsed valves to release a brief burst of reagent gas has been shown to further reduce the gas load on the FT-ICR system (2).

Laser Desorption

LD ionization has emerged as the most popular and successful approach for producing ions from low-volatility solid samples and has been widely recognized as being especially well matched to the FT-ICR analyzer. It is relatively easy to transport the laser pulse into the ICR cell region; depending on geometry, either nothing needs to be placed in high vacuum except the sample probe or at most a small number of mirrors and/or lenses. The pulsed nature of the laser (usually at repetition rates below 10 Hz) matches well with the cyclical nature of the FT-ICR MS experiment. The laser beam itself introduces no gas load to the

system, and the transient burst of neutral species coming from the sample surface is pumped away before FT detection.

IR (CO_2), visible (Nd:YAG) and UV (Nd:YAG, excimer) lasers have all been successfully used for LD. At fluences of the order of 10^2 J/cm^2 or intensities of 10^9 W/cm^2 each laser shot produces observable cratering of the surface and a dense, hot plasma plume. Neutrals predominate, and the ionization mode is largely thermal. A substantial amount of chemistry occurs as the plume expands. Ion-neutral adducts are often formed, and ionization of neutrals of low ionization potential (such as alkali atoms) is enhanced far above their proportional abundance. Chapter 6 provides a further discussion of some of the current models for LD sample ionization.

Multiphoton Ionization

Multiphoton Ionization (MPI) is an approach for ionizing volatile samples with some striking advantages in selectivity over EI. This technique was first demonstrated in FT-ICR MS by Irion et al. (3) using a UV excimer laser. In MPI, an intense pulse of UV or visible light is used to ionize gaseous neutrals within the ICR cell. The neutral molecule must absorb two or more photons to reach its ionization threshold. One recent analytically oriented study used MPI for the ionization of a gas chromatographic (GC) effluent (4). The authors obtained detection limits of 7 pg for naphthalene and demonstrated the selective ionization of aromatics in gasoline. Variation of both the laser wavelength and the laser power density present promising possibilities for selective, high-information-content analyses.

Secondary Ion Mass Spectrometry

Secondary ion mass spectrometry (SIMS) as an ionization approach is challenging because of the difficulty of introducing the ionizing ion beam into the magnetic field. Castro and Russell at Texas A&M (5,6) overcame this problem with an ingeniously designed cesium ion gun residing within the high-field region, but this has not been widely employed. Another approach reported by Amster et al. (7,8) has been to place the ion gun outside the high-field region and direct the ion beam along the field lines through the cell, striking the sample probe tip at the other end of the cell. Kellerhals and Allemann (9) developed a SIMS technique specifically adapted to the geometry of an ICR cell in which primary ions trapped in the cell are accelerated by an rf pulse and directed onto the sample surface mounted on a probe that extends into the cell; however, this development has been superseded by external-source technology. Liquid SIMS (with, for example, a glycerol sample matrix) does not match well with the vacuum requirements of the ICR cell and has not been developed.

Fast Atom Bombardment

The related fast atom bombardment (FAB) ionization approach would seem to be better suited to the FT-ICR MS circumstances, because the ionizing neutral beam can be produced outside the magnet and then passed without difficulty into the high-field region. This has not been a common approach, however, because of the relatively high vapor pressure of typical FAB matrices (e.g., glycerol) and the large distance (typically exceeding 50 cm) over which a collimated neutral beam must be transported. Hill and Marshall have used a nontraditional FAB source (technically the projectile is a *fast neutral molecule*) to circumvent the latter problem (10). An SF_6^- ion gun is used to produce high-energy ions that can be collimated into a fine beam. The SF_6^- spontaneously undergoes autoneutralization (loses an electron) before entering the magnet field region. The beam diverges to less than 1 mm diameter while traveling approximately 1.5 m to the cell. Spectra have been obtained for Teflon, a nonconducting polymer, with this source (11).

Plasma Desorption

Plasma desorption (PD), also known as ^{252}Cf ionization, is an effective technique for very high-molecular-weight samples. The typically low rate of ion production is effectively compensated in FT-ICR MS by accumulating ions for a long time in the trap. In typical configurations, the ^{252}Cf is placed behind a thin foil that has the sample deposited on the front side. The assembly is mounted on a probe that is moved adjacent to the trapped-ion cell. Ions can be accumulated over a period ranging from seconds to several minutes before the detection sequence (12–15).

Desorption–Ionization Variations

Several hybrid desorption–ionization techniques have been reported that use a desorption step followed by a different, more efficient ionization step. Additional sensitivity arises because one-step desorption/ionization techniques (e.g., LD ionization) are very inefficient; typically 1000 neutrals are desorbed for every ion. In hybrid desorption–ionization techniques, the second step is used to ionize the large number of gas-phase neutrals produced during desorption. Not all combinations that have been reported in MS have been conducted with an FT-ICR MS. Those reported to date for FT-ICR MS include LD/EI, LD of sample neutrals/CI, and LD of reagent ions/CI. LD/MPI (16) and sputtered neutral using an ion gun/MPI (17) have been reported on time-of-flight instruments.

LD/EI ionization has been reported for polymer additives (18) and adsorbed reaction intermediates on a catalytic surface (19). Hsu and

Marshall (18) compared LD ionization with LD/EI ionization for detecting a dye in poly(methyl methacrylate). The signal-to-noise ratio of the LD/EI spectrum was significantly better than the LD-only spectrum. The dye was detected as a poly(methyl methacrylate) adduct ion at a concentration of 0.1% in the poly(methyl methacrylate), improving the detection limit of the dye by an order of magnitude over attenuated total-reflectance IR spectroscopy.

McIver, Hemminger and coworkers have used a mild excimer laser pulse to desorb neutral sample molecules from a cold platinum crystal surface with EI of the desorbed molecules (19). In this study, the chemistry occurring with cyclohexane on the platinum surface was monitored by using the laser to sample the surface-bound molecules as a function of surface temperature, showing the intermediate species formed on the way to benzene. This application demonstrates the potential of LD/EI ionization for observing adsorbed reaction intermediates on catalytic surfaces. This technique has also been used to identify silicone oil contaminant on magnetic storage media (20).

McIver, Hemminger and coworkers have also explored LD with subsequent CI, which is particularly suited to the ICR trap. In one approach to LD/CI, a population of reagent ions is first produced by EI of methane and trapped in the cell (21). A laser pulse is then used to desorb sample molecules from a surface. The sample molecules traverse the center of the trap and are ionized by the reagent ions after which selective ion ejection pulses purge the cell of unreacted reagent ions. Sufficient CI of the sample molecules is achieved during their single pass across the trap to give excellent FT-ICR signals, as was demonstrated for samples of pentadecylacridine and thymidine.

A technique pioneered by Freiser and co-workers uses LD ionization of metal surfaces to generate metal ions whose reactions with neutral organic and inorganic molecules have been extensively explored (22,23). Having been freed from the restriction of using metallic reactant ions derived from the small catalog of volatile inorganic compounds, gas-phase chemistry of metal-containing ions has experienced a tremendous surge of development.

External Source Ionization

As suggested at the beginning, there are no evident barriers to coupling the known ion-source technologies to an external-source FT-ICR MS. All of the common ionization techniques have been demonstrated with FT-ICR external sources. Particularly important to the analytical chemist is the use of thermospray by Stockton et al. (see Chapter 9) and electrospray ionization (24,25), which effectively ionize the effluent of a liquid chromatograph (LC), and continuous-flow FAB, offered by Spectrospin (see Chapter 4). These techniques use the high-resolution, high-mass accuracy capabilities of FT-ICR MS on thermally labile, higher-

molecular-weight samples best introduced in solution. In most cases, the ion sources can be of conventional design, and the uniqueness of the setup is in the hardware used to transport ions from the ion source to the cell. This is discussed further under Differentially Pumped Configurations.

Ion Activation and MS/MS

In this section, we refer to ion activation as the process of imparting energy to primary ions in order to produce fragmentation. An MS/MS experiment uses the primary ion/product ion correlation in several ways. In one MS/MS experiment, the identity of the product ions simply yields structural information on the parent ion. In another type of MS/MS experiment, all primary ions yielding a structurally significant product ion are identified. The information gained is that the primary ions will all be related by a structural feature. A third MS/MS experiment is the *neutral loss* experiment, where all primary ions losing a certain neutral fragment are identified. In this case, the neutral fragment that is lost is the structural tie between the primary ions. The latter two types of MS/MS experiments have traditionally been conducted on two-stage spatially separated analyzers, such as triple quadrupole or sector–sector configurations.

The experiment identifying the product ions of a single primary ion is the most frequently used analysis and can be conducted on any tandem MS arrangement. This is the MS/MS experiment typically conducted by FT-ICR MS, where the "mass-spectrometers" are temporally separated. FT-ICR MS has the additional advantages of product ion detection at high resolution and high-mass accuracy. Either collisional activation (CA) or photon absorption can be used to induce fragmentation. Photon absorption to produce photodissociation is particularly well suited to trapped-ion analyzers such as FT-ICR MS or quadrupole ion traps, because low photon flux sources can be used in conjunction with long exposure times. These experiments as conducted in FT-ICR MS are described in the remainder of this section.

Collisional Activation and Collision-Induced Dissociation

An ion excited to a large-diameter cyclotron parking orbit has substantial velocities, and a subsequent collision with a neutral gas molecule can cause collision-induced dissociation (CID) with considerable energy deposition in the ion. For instance, an ion of mass 200 in a 1-cm-radius orbit in a 3-T field has a kinetic energy of about 200 eV. Other typical ion energies for a 6-T mangetic field are listed in Table 2.1. Such energies are higher than in the widely used low-enery MS/MS in "tandem quadrople" instruments. Performing MS/MS in the FT-ICR cell benefits from the ease of selectively exciting just one single ion mass so

Table 2.1 Kinetic Energy (*KE*) versus Cyclotron Radius at 6-T Magnetic Field

Radius (mm)	Kinetic Energy (ev)		
	m/z 28	m/z 280	m/z 2800
1	61	6.1	0.61
3	550	55	5.5
10	6150	615	61.5
30	55 keV	5500	550

$$KE\ (\mathrm{J}) = \frac{(eBr)^2}{2M} \quad \text{(SI)}$$

$$KE\ (\mathrm{eV}) = 47.8\,\frac{B^2r^2}{M} \quad \text{(T, mm, Da)}$$

that the CID spectrum of any chosen species in the cell is immediately available.

Some of the most dramatic and promising MS/MS applications in FT-ICR MS involve sequential dissociations in which successive fragmentation of the initial ion into smaller and smaller fragments is followed by a series of excitation/observation steps on the successive fragments (26,27). This idea was strikingly demonstrated by Freiser's group at Purdue (28) who showed MS/MS/MS results for parent ions of acetophenone and nitrotoluene and a reaction–product ion from acetic anhydride. A recent excellent illustration of MS^n analysis is shown in Figure 2.1, where five CID steps are used, along with selective ejection, to proceed from $[FeS_{10}]^+$ all the way to Fe^+ (29). Carrying such multiple MS/MS observations to four or five steps is basically equivalent to a multisector or multiquadrupole MS/MS experiment using a long (and impractical) series of sectors or quadrupoles.

The above experiment illustrates the use of an FT-ICR MS as a series of temporally separated mass analyzers. Recent work (29–32) has also demonstrated the spatial separation of mass analysis using a dual-cell FT-ICR MS configuration (described under Differentially Pumped Configurations). Spatial separation can serve to isolate the analyte ions from neutrals involved in their formation or to transfer the ions to a region where another reagent or collision gas is present. In the basic implementation of this technique (30), all ions except those of the desired mass are excited into a cyclotron orbit slightly larger than the orifice between the two cells. The trapping potential of the dividing trap plate is then dropped to allow the selected ions to pass into the opposite cell. In more sophisticated implementations by Hanson et al. (31) and Farrell et al. (32), all ions are excited to larger-diameter orbits and then the selected ions are deexcited and allowed to pass into the opposite cell.

FT-ICR MS is capable of high-resolution and high mass accuracy

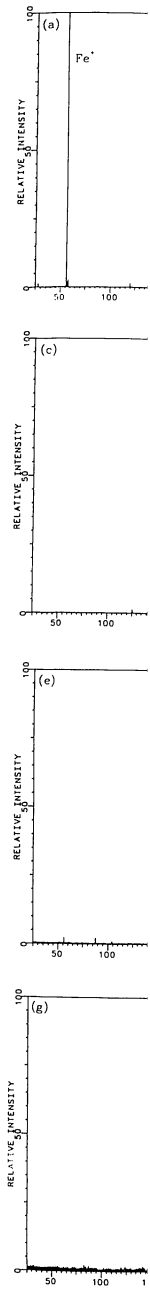

Figure 2.1 An
laser desorptic
(c) Isolation o
Isolation of Fe
of FeS_2^+. (*l*) C

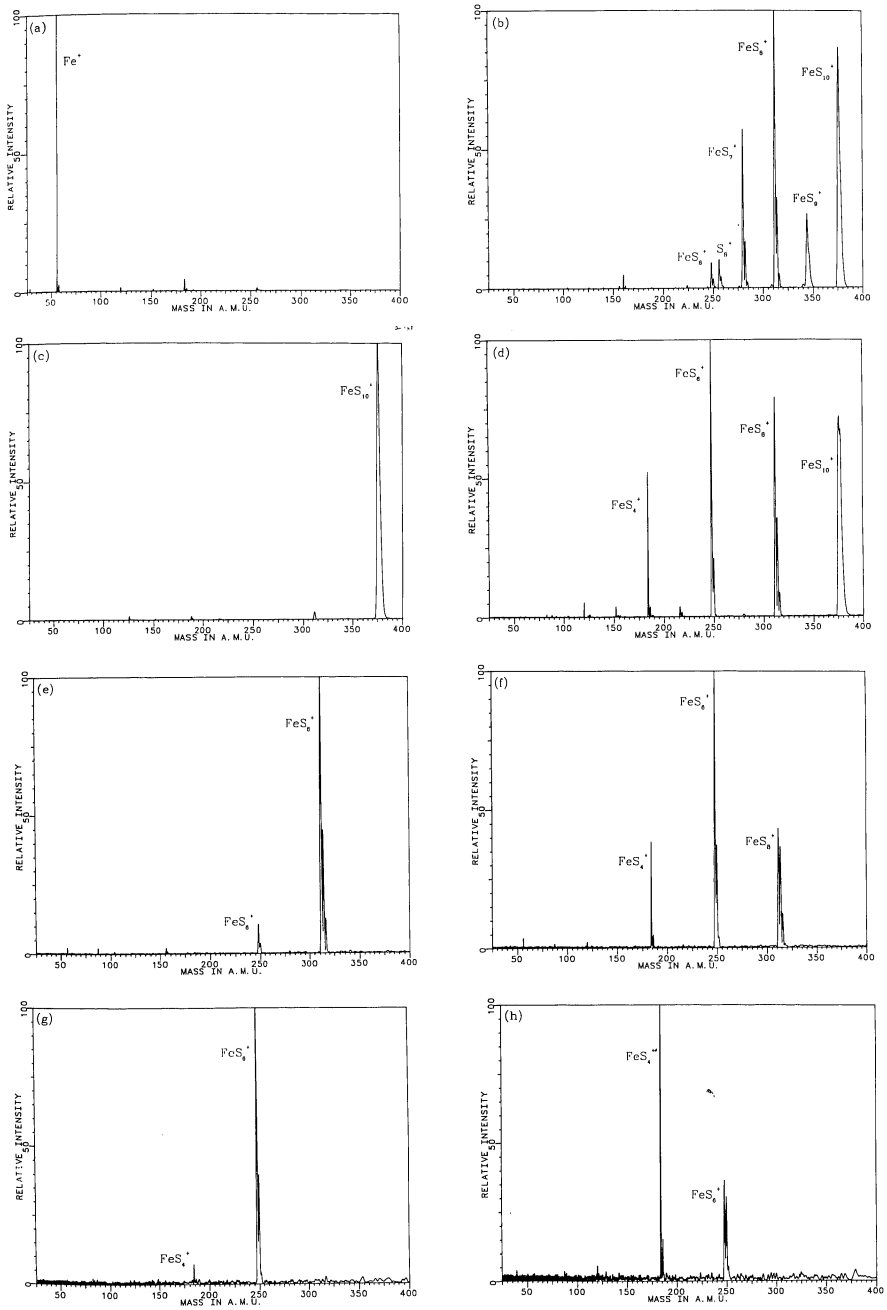

Figure 2.1 An example of a multiple MS/MS experiment. (*a*) Isolation of Fe^+ following laser desorption and collisional cooling with argon and S_8. (*b*) Reaction of Fe^+ with S_8. (*c*) Isolation of FeS_{10}^+. (*d*) CID of FeS_{10}^+. (*e*) Isolation of FeS_8^+. (*f*) CID of FeS_8^+. (*g*) Isolation of FeS_6^+. (*h*) CID of FeS_6^+. (*i*) Isolation of FeS_4^+. (*j*) CID of FeS_4^+. (*k*) Isolation of FeS_2^+. (*l*) CID of FeS_2^+. (Reprinted with permission from Ref. 29.)

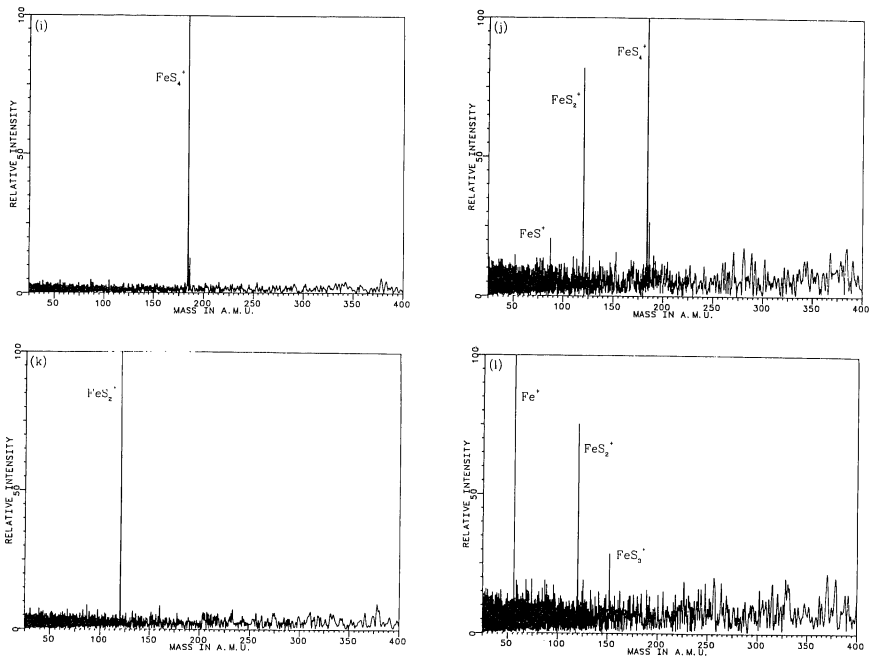

Figure 2.1 (*Continued*)

product ion detection. By using a pulsed valve for collision gas introduction, Cody (33) was able to measure masses of up to 350 Da with a mass accuracy of better than 10 ppm. In an experiment using the high-pressure region of a dual cell for collision gas and the low-pressure region for detection, Wise (34) was able to obtain a resolution of 20 000 at m/z 105.

Photodissociation

Photon absorption leads to fragmentation and provides several kinds of analytically useful information (35,36). One approach is to use the fragmentation pattern from photodissociation of a primary ion as a secondary mass spectrum (the photodissociation mass spectrum). As an alternative to CID for characterizing ions of unknown structure, such a photodissociation mass spectrum has the advantage that it can be obtained at arbitrarily low pressure without collision gas and without disturbing the ion motion. With far-UV laser sources like the ArF excimer laser, photon absorption deposits a large and uniform amount of energy in the ion of the order of 6 eV, which can be more effective than low-energy CID in producing useful fragmentation. As one recent illustration of the use of photodissociation mass spectra, Bowers et al. (37) have taken advantage of the strong light absorption of polypeptides

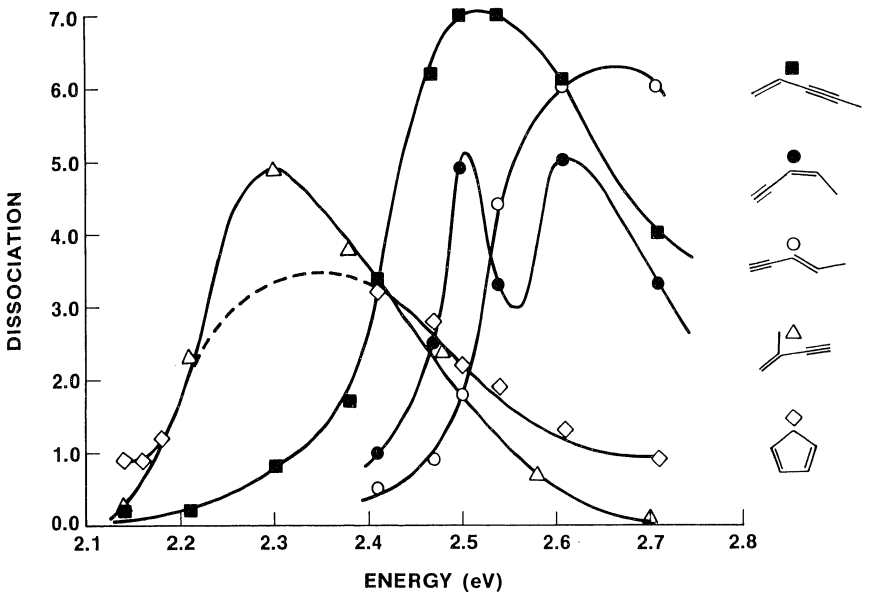

Figure 2.2 The photodissociation of C_5H_6 isomers. Values plotted for cyclopentadiene are 10 times measured values.

around 193 nm to obtain useful secondary photofragmentation patterns of polypeptide ions, leading to sequence information about the parent polypeptide. A detailed example of this application is presented in Chapter 8.

Another approach for characterizing ions by using photodissociation is the technique of photodissociation spectroscopy (PDS) (35). PDS uses the wavelength dependence of the photodissociation rate to give a wavelength spectrum characteristic of the ion. This is useful as a delicate way of distinguishing isomeric ions. An example of this idea is shown in Figure 2.2, using the wavelengths available from an argon-ion laser, where the photodissociation spectra of five different isomers of $[C_5H_6]^+$ are shown to have very different PDS spectra (38). This is a useful "fingerprinting" approach to characterizing ion structures.

Excitation and Detection

In conventional beam-type mass spectrometers, high performance is achieved by designing ion optics and mass analyzers to give maximum transmission of desired ions combined with maximum discrimination against ions nearby in mass. The actual ion detection is straightforward and detector sensitivity is not a problem, because single-ion detection by electron multipliers is routine. High-performance FT-ICR detection

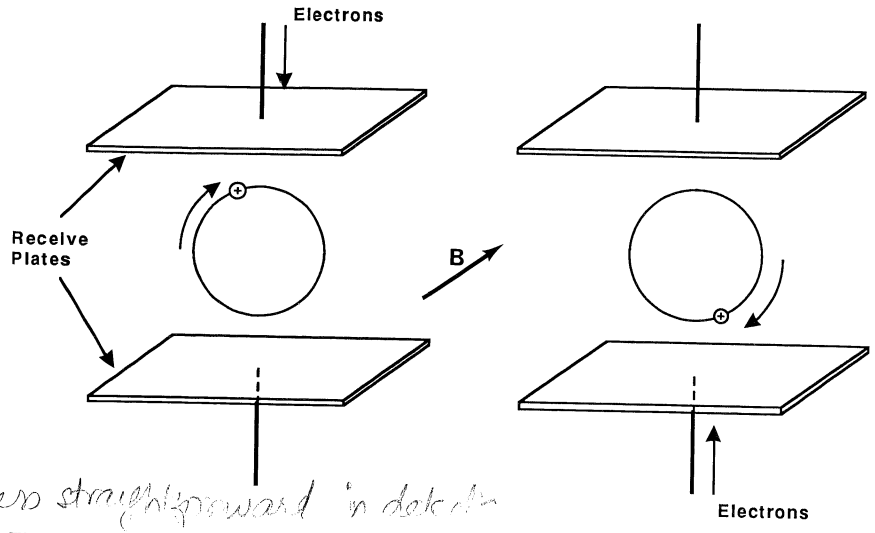

Figure 2.3 A rotating monopole description of signal generation. Circulating charges induce a current that is detected by a differential amplifer as *V*.

is less straightforward, and the technology is still in the process of intense development. Challenging problems arise, first, because the ion motions in the three-dimensional ICR cell are complex and coupled in nonlinear ways; second, because detection is detector-noise limited (the signal from a single ion being below the detector noise level); and third, because of the numerous methods that can be used to process the signal information (39).

Comisarow (40) discussed the principle of ICR detection in terms of a *rotating monopole* model (Figure 2.3). As the ion circulates in its cyclotron orbit, it alternates between being close to the upper receiver plate (Figure 2.3, *left*) and the lower receiver plate (Figure 2.3, *right*). When it is close to the upper plate it induces an image current on the plate (drawing negative charge from the lower plate through the connecting circuit). Conversely, when the ion moves near the lower plate, the image current induced on the lower plate draws negative charge through the circuit from the upper plate. The result is an alternating current flowing through the detector electronics at the cyclotron frequency of the ion.

Following this illustration, the amplitude of the signal increases with cyclotron radius up to the point where the radius is equal to the half-distance between the receiver plates at which point the signal current per ion corresponds to one full electron of charge oscillating between the receiver electrodes. To obtain a flat spectrum without mass discrimination, all ions should be excited to the same cyclotron radius. Because the radius is given by

$$R_c = Et/B \qquad (2.1)$$

where E is the excitation rf amplitude, t is the duration of the excitation pulse, and $\boldsymbol{B}$ is the magnetic field; a flat spectrum should result if each ion experiences an rf pulse of the same duration and amplitude.

In his classic paper (40), Comisarow derived a series of signal-modeling equations for ICR detection based on a "cell" consisting of a pair of infinite, parallel detector plates. The calculation of signals for ions in real cells of various geometries is more complex. It was found that this can be done easily in general by applying the *reciprocity theorem* (41). This says that the image charge created by an ion on a detector plate is proportional to the electrostatic potential that is created at the position of the ion by applying a voltage of 1 V to the detector plate in the absence of the ion. Because the latter is easily calculated by numerical solution of Laplace's equation, FT-ICR signal strengths are readily calculated.

The amplitude of the signal per ion does not depend on the size of the cell, but only on the ratio between the radius of the cyclotron orbit and the distance between the receiver plates. Larger cells can increase the signal amplitude because they can trap more ions, but an increase in size does not affect the signal amplitude per ion.

Although all steps from ion excitation to final spectrum generation are coupled and strongly interdependent, it is helpful to think separately about (1) ion excitation, (2) signal acquisition, and (3) information processing.

Ion Excitation

The first step in FT-ICR MS detection is to "spin up," or accelerate, the ions of interest into large cyclotron orbits. This also separates the ions into distinct ion packets of different mass-to-charge ratios. Usually the goal is excite all ions in the mass spectral range of interest to the same cyclotron orbit radius to give a flat spectrum without mass discrimination. At the same time, one may want to leave some ions unexcited, because space-charge (Coulomb repulsion) interactions lead to severe problems if the number of ions in the cyclotron parking orbit is large. In addition, the same excitation source may be used for ion ejection sequences before the detection sequence begins and also for excitation of selected ions into large, but nonejecting orbits for MS/MS applications. These ejections and excitations should be efficient, versatile, and selective.

Several approaches to ion excitation have been used, achieving these goals to varying degrees. The effects of an excitation waveform can be evaluated by displaying the excitation spectrum. This is obtained by performing a FT on the time-domain excitation waveform. The excitation spectrum shows the amount of excitation at any frequency or mass, from which parameters such as ion radius, ion excitation energy for MS/MS, and overall evenness of the excitation can be observed.

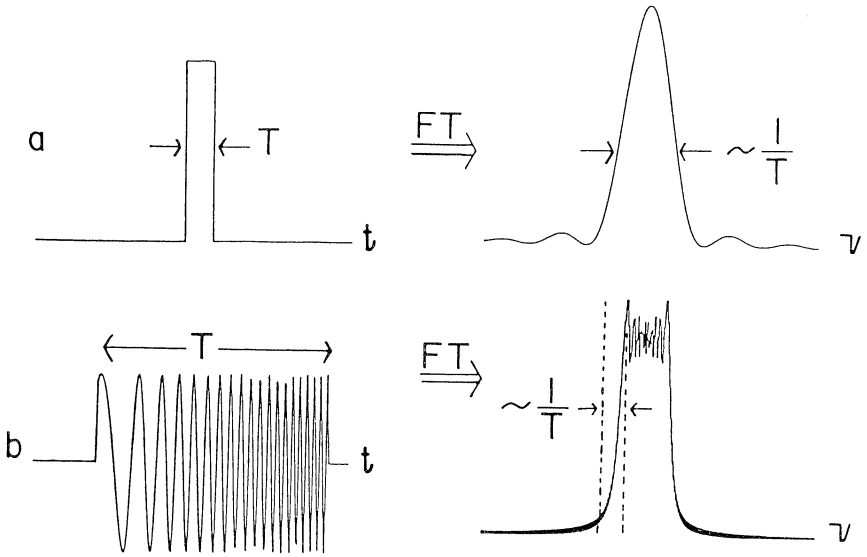

Figure 2.4 A Fourier excitation waveform and excitation spectrum for impulse (*a*) and chirp (*b*) excitation. (Reprinted with permission from Ref. 46.)

Impulse Excitation

An ideal delta function pulse (infinite amplitude, zero width) has a flat excitation spectrum and should excite all ions equally. In real-world approaches to this ideal a pulse of finite width and height is used (Figure 2.4*a*): The shape of the pulse is not very important. The mass range of ions that are excited extends from infinite mass to a lower-limit mass whose angular cyclotron frequency is of the order of $\omega_{c,max} = 1/t$, where t is the pulse width. McIver et al. (42) have discussed the quantitative aspects of impulse excitation and have shown that it is useful with a pulse amplifier delivering peak pulse amplitudes of the order of 1 kV (43).

Chirp Excitation

The most commonly used excitation waveform is the chirp, an rf pulse whose frequency sweeps rapidly over the range from the lowest to the highest (or vice versa) frequencies desired in the spectrum (Figure 2.4*b*) (44). A fairly flat excitation spectrum results if the frequency sweep traverses a constant number of Hertz per second. The mathematics of the FT with a chirp are slightly complicated, but were formulated long ago (see Ref. 39). The advantages of chirp excitation are its rather simple implementation and the ease with which a wide mass range can be

excited without the need for large rf amplitudes and expensive amplifiers. Disadvantages are the somewhat nonuniform excitation of the ions, which becomes pronounced for ions near the edge of the swept frequency range (as observed in Figure 2.4*b*); the fact that the final cyclotron radius is limited to less than the full-cell dimension due to the excursion above the final radius that the ion experiences during the chirp; and the fact that different ion masses are accelerated at different times, which can introduce peak height distortions due to space-charge interactions. Axial ion ejection at frequencies slightly above an ion's cyclotron frequency also may be a problem (45).

SWIFT

In 1985, Marshall's group introduced the method that they termed *stored waveform inverse Fourier transform* (SWIFT) excitation, which is the most satisfactory approach to achieving complete control over the excitation characteristics (46–48). It is based on the principle that the excitation actually experienced by each ion and, hence, its final radius is proportional to the amplitude of the excitation spectrum (more precisely the Fourier power spectrum) at its frequency. Recalling that the excitation spectrum is produced via a FT of the excitation waveform, a desired excitation waveform can be produced via an inverse FT of the excitation spectrum. The SWIFT concept is to specify first the excitation spectrum actually desired for the excitation waveform. This would usually be a square shape covering the desired frequency range, as in Figure 2.5*a*. It can, however, just as well be a complicated shape with gaps, changing amplitudes, and other features (Figure 2.6). The specified excitation spectrum is inverse Fourier-transformed to give the time-domain excitation waveform, as in Figure 2.5*b*. If carried out precisely, this gives an excitation waveform that will excite each ion species to exactly its preselected cyclotron radius. For some ions this radius may be larger than the cell dimensions, selectively ejecting these ions; for some it may be zero, giving no effect; and for others it may be the cyclotron radius appropriate for FT-ICR detection.

In its simplest form, the SWIFT procedure results in waveforms with inconveniently large peak voltages for the rf excitation amplifier. However, there is flexibility in that an infinite number of different time-domain waveforms can be chosen to yield any specified frequency-domain excitation power spectrum. Recent SWIFT implementations have taken advantage of this flexibility to even out the amplitude of the time-domain waveform. At the cost of some instrumental complexity, current SWIFT implementations give a high degree of precision and flexibility to the ion excitation process. The advantages of this approach are so great that it will probably replace other excitation methods in all but specialized applications.

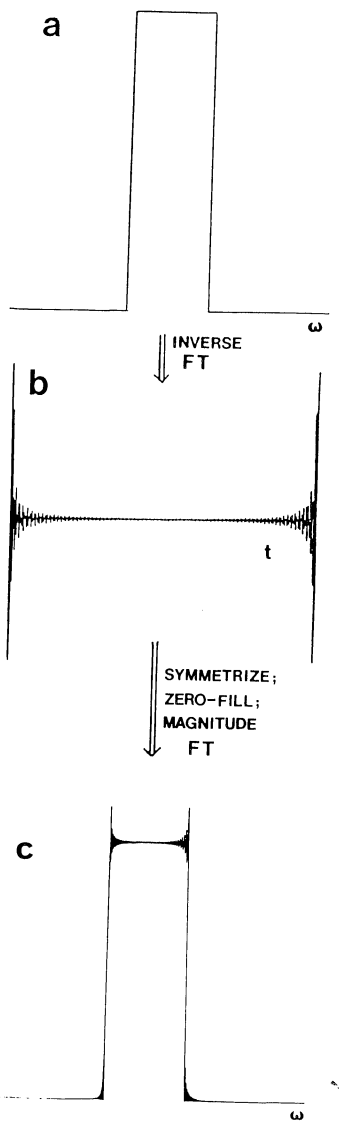

Figure 2.5 The SWIFT excitation waveform is generated by taking the desired frequency spectrum (*a*) (power as a function of frequency) and performing an inverse FT to give a time-domain signal (*b*). This waveform is then generated by a digital frequency synthesizer. The excitation spectrum (*c*), which indicates the actual amount of power applied at each frequency, is produced by Fourier transformation of *b*. Note how even the excitation spectrum is compared to chirp excitation (Figure 2.4b) (Reprinted with permission from Ref. 46.)

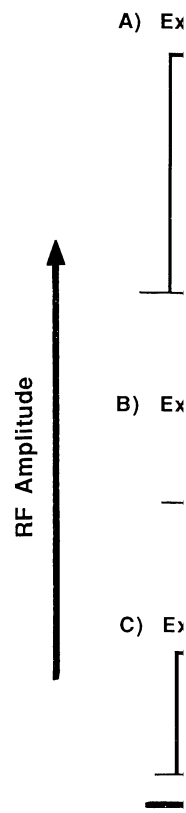

Figure 2.6 An ex
applied in a CID
Fourier tranforma
will eject all mas
waveform which
spectrum of a m
mass range.

Signal Acqu

For a typical
preamplifier i
low-noise elec
ature about th
tion of this sig
signal is norma
noise, low-inp
response exter

If the spectr
Da), the time-d

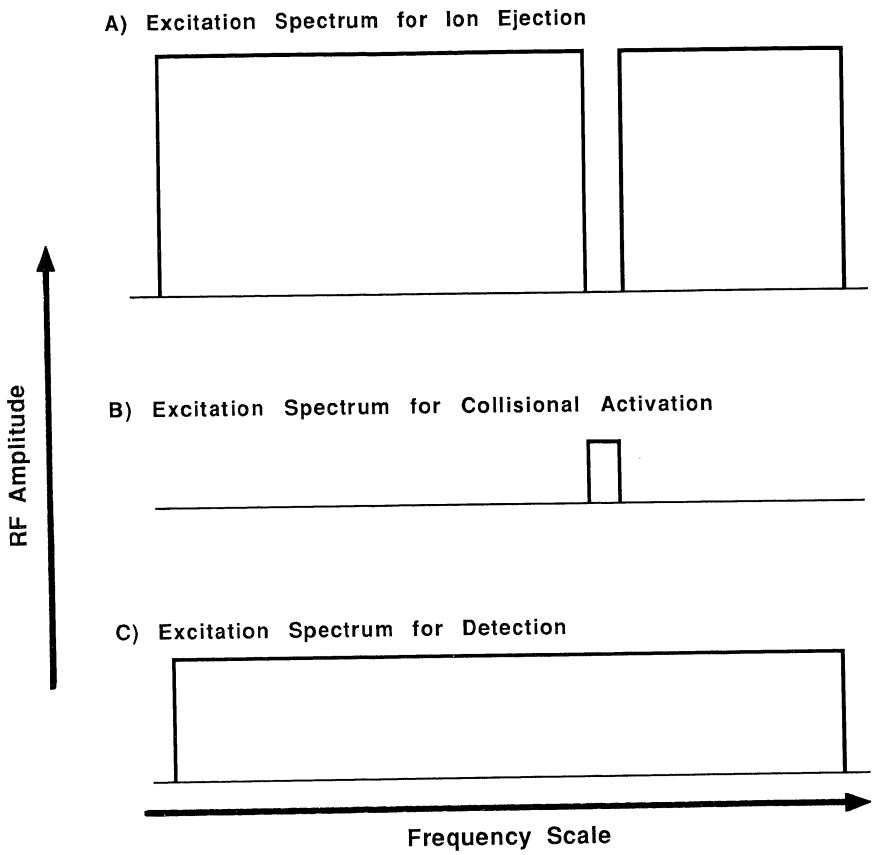

Figure 2.6 An example of a series of SWIFT excitation spectra for the waveforms that are applied in a CID experiment. The waveforms actually used are produced by inverse Fourier tranformation of the excitation spectra. Applying a waveform with spectrum *a* will eject all masses except the mass of interest. *b* is the spectrum of a lower amplitude waveform which applies some collisional energy only to the ion of interest. *c* is the spectrum of a medium amplitude excitation waveform for detection across the entire mass range.

Signal Acquisition

For a typical ion cloud of 1000 ions, the rf signal appearing at the preamplifier input is of the order of a few hundred microvolts, so that low-noise electronic design is very important. There is substantial literature about the characteristics, noise levels, and techniques of acquisition of this signal voltage. The amplifier (usually differential, because signal is normally acquired from both receiver plates) needs to be a low-noise, low-input-capacitance, broadband amplifier with a frequency response extending up to at least a few megahertz.

If the spectrum includes ions at fairly low masses (below 50 or 100 Da), the time-domain signal will include frequencies in the megahertz

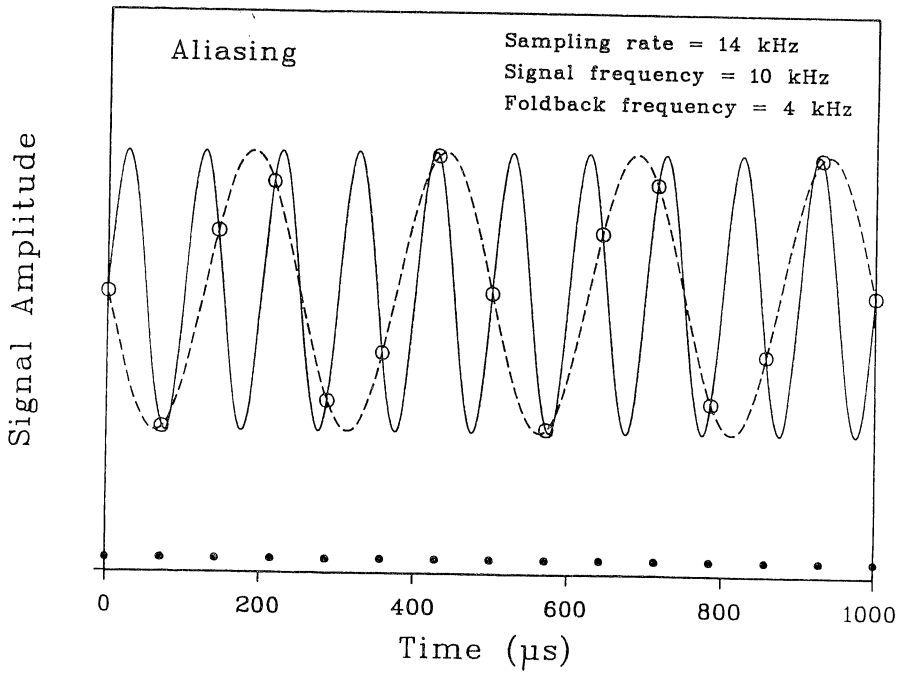

Figure 2.7 The aliasing phenomenon. The signal being acquired is at 10 kHz (solid curve), while the A/D converter samples at 14 kHz (as shown by the dots along the time axis). It is clear that the sampled points (open circles) are identical to what would be observed if we were sampling a signal at 4 kHz (dashed line), which is the foldback frequency from equation 2.3. This signal thus appears in the Fourier spectrum as a foldback peak at 4 kHz.

range and providing sufficient computer memory to store a long transient is a serious concern. The rate at which the signal must be sampled and stored is governed by the *Nyquist criterion*, which states that the sample rate f_s must be faster than twice the highest frequency being acquired in the time-domain signal. If the spectrum includes an ion whose frequency f_{cyc} is greater than the Nyquist limit, $f_{nyq} = f_s/2$, then the phenomenon of *aliasing*, or *folding back*, is observed. A foldback peak appears in the FT spectrum at a lower frequency f_{fb}, given by

$$f_{fb} = f_s - f_{cyc} \tag{2.2}$$

where f_s is the sampling frequency. If f_{cyc} is greater than f_s, then the more general equation

$$f_{fb} = |nf_s - f_{cyc}| \tag{2.3}$$

applies, where n is an integer chosen so that f_{fb} lies in the range from zero to $f_s/2$.

Figure 2.7 illustrates how in the aliasing situation a frequency (10 kHz) that is higher than the Nyquist limit (7 kHz) appears in the

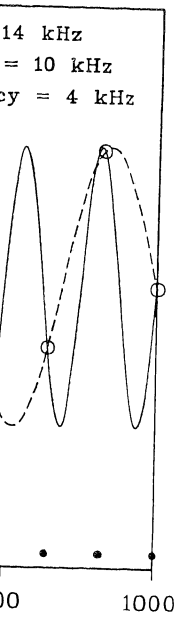

t 10 kHz (solid
s along the time
what would be
is the foldback
spectrum as a

a long tran-
t be sampled
ates that the
uency being
udes an ion
$= f_s/2$, then
A foldback
given by

(2.2)

f_s, then the

(2.3)

range from

quency (10
ears in the

sampled spectrum to be indistinguishable from a true signal at the foldback frequency (4 kHz).

Full Spectrum Mode

Signals may be acquired in either full-spectrum (sometimes call *broadband*) mode or heterodyne (sometimes called *narrowband* or *mixed*) mode. In full-spectrum operation, the signal from the preamplifier is sampled directly by the analog-to-digital (A/D) converter at a rate greater than or equal to the Nyquist limit for the lowest-mass ion to be observed. Unless low-pass filtering is used, ions of lower mass than this limit will appear as foldback peaks in the spectrum. The sampled time-domain signal is stored for transforming. When the experiment permits repeated transients from the same sample, the spectrum is usually signal-averaged by summing the time-domain transients from all repetitions in the same space in memory before performing the Fourier transformation.

Heterodyne Mode

In order to extract the maximum amount of resolution information from the ICR signal, it is necessary to sample for the duration of the signal. The Nyquist limit must also be observed, requiring acquisition rates of tens of kilohertz to megahertz for typical masses. At these rates, an inordinate amount of buffered memory is needed to acquire a signal lasting seconds. Heterodyning is used to shift a narrow range of sample frequencies to the audio range so that slower aquisition rates can be used. In the heterodyne mode, the signal from the receiver plates is first mixed with a reference signal at, for example, a frequency f; the sum and difference frequencies from this mixing or heterodyning go through a low-pass filter (cutting off typically at a few kilohertz) to reject the sum frequencies (Figure 2.8). The result is to shift a narrow band of signal frequencies centered at f down to the audio frequency range. These are passed to the A/D converter, while the signals from all ions outside this narrow range are discarded. The remaining signal, now confined to audio frequencies and, hence, presenting low data acquisition rates, is sampled at a low frequency for a long time (up to several seconds in the highest-resolution applications) and stored. The mass resolution over the narrow spectral range displayed is a factor of s_b/s_n higher than the broadband mass resolution of the original spectrum, where s_n is the sampling rate in the narrowband acquisition and s_b is the sampling rate that would be used to acquire the same transient in broadband mode, assuming the same number of data points are acquired in each case. This illustrates the principle that the available mass resolution increases directly with the observation time. (This principle and the possibility of enhancing mass resolution by narrow-

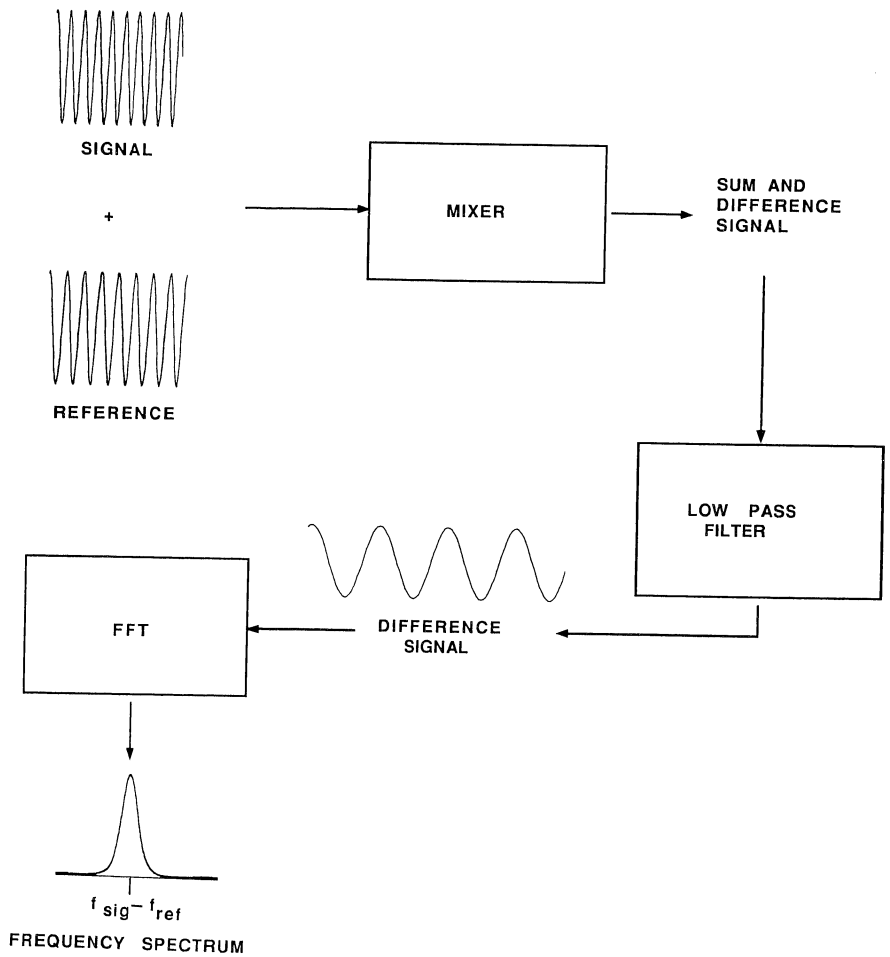

Figure 2.8 A description of narrowband acquisition through signal heterodyning. The sample signal is mixed with a reference signal. This results in a signal that contains both the sum and difference ("beat") frequencies. A low-pass filter is used to eliminate the high-frequency component. In order to take advantage of the entire signal transient, the low frequency can be sampled at slow rates for a period of seconds. The FT of this waveform produces a peak at the difference frequency.

band detection only apply to the extent that the peak widths are limited by acquisition time and not by other line-broadening mechanisms (see Resolution).)

Data Processing

The time-domain signal consists of a sum of decaying oscillations at the cyclotron frequencies of all the excited ions, whose decay time constants reflect the spectral widths of the peaks. In the absence of noise,

straightforward Fourier transformation of this signal would give the mass spectrum. Noise arises from several sources: the front-end stages of the preamplifier produce electrical (Johnston) noise, the sampling process with a finite number of bits produces digitization noise (as well as truncation noise when the A/D converter overflows on strong signal excursions), and the fact that a typical peak corresponds to only 10^2–10^5 individual ions introduces statistical-fluctuation noise. Because the sensitivity and the dynamic range of the spectrometer depend on maximizing the signal-to-noise ratio, much of the effort in developing transform methods in FT-ICR has been directed at optimizing the extraction of weak ICR peaks from the noisy signal.

Given a time-domain spectrum consisting of N points, where N is typically between 16 K and 128 K, it is common to zero-fill at least once, apodize, and take the magnitude-mode FT with a FFT algorithm. One zero fill (adding N zeros to the end of the data set) increases the signal-to-noise ratio and increases the displayed resolution of the spectrum; further zero filling has the effect of line smoothing, but adds no information to the spectrum (39).

In order to modify spectral properties such as signal-to-noise ratio, resolution, and peak shape, the data set is multiplied by an *apodization*, or window, function (49–51). In NMR, the apodization function can be used to weight the front end of the data set where the signal-to-noise ratio is higher to improve the signal-to-noise of the transformed spectrum. Conversely, the latter part of the data set can be enhanced, increasing the certainty of the frequency and, hence, the resolution at the expense of signal-to-noise. In FT-ICR MS, the apodization function is used more commonly to minimize artifacts of the Fourier transformation such as side lobes that arise because of the finite nature of the data set.

A *magnitude-mode* FT is most frequently used. Although the magnitude-mode transform produces broader peaks than the *absorption-mode* transform, it avoids the problems of phase variations across the spectrum, which are difficult to eliminate entirely. The availability of economical array processors has reduced the computation time for even large transforms to a fraction of a second. In a modern instrument incorporating this capability, the delay between the end of a transient acquisition and the availability of the frequency-domain spectrum can be so small that the instrument appears to acquire frequency-domain spectra in real time.

The straightforward FT is a completely rigorous, well-determined way to convert a time-domain transient into a frequency-domain spectrum under the conditions that (1) the time-domain signal is a linear and undistorted reflection of the individual ion cyclotron motions, (2) no prior knowledge of the form the frequency-domain spectrum will take is assumed, and (3) there is no noise. These assumptions are not totally realistic: various nonlinear ion motions and couplings between

ions, as well as signal-processing nonlinearities, lead to nonlinear behavior. Actually, a lot is known a priori about the form of the spectrum, in particular, that it will consist of several peaks of similar widths and approximately Lorentzian lineshape, and the presence of noise in the time-domain transient means that many different frequency-domain spectra are consistent with the observed transient within the limits of the noise. Considerable thought has gone into using more sophisticated information-processing methods to extract useful spectral information more effectively from the observed transients. A simple illustration of using a priori knowledge of the spectrum is the procedure of replacing the latter part of the transient with zeros in a case where a transient dies away below the noise level before the end of the acquisition time. By replacing a segment of the noisy transient that we know to be nearly zero with true zeros, only a small amount of information and a large amount of noise is eliminated, and the net signal-to-noise ratio is improved. (Note that this is not the same as zero filling, which subtracts neither information nor noise from the data.)

Several advanced processing methods have been explored. The method of segmented Fourier transformation (52,53) (called SEFT by the Amsterdam group) divides the transient into sections and makes a fit to equations that incorporates the known Lorentzian character of the peak shapes. This procedure gives significant improvements in relative peak heights and resolution without major increases in computation.

Other transformations besides Fourier transformation can offer advantages. The Hartley transform was explored by Williams and Marshall (54) and the Hadamard transform by McLafferty's group (55), but these have not been used much in practice. Methods have also been explored for bringing to bear powerful probabilistic methods to derive the "best" frequency domain spectrum compatible with the data, which include the very general approach of Bayesian transformation (56) and the special case known as the *maximum entropy method* (39,57). These latter methods yield very impressive results in terms of pulling reliable spectra out of small, noisy data sets, but are very costly in computation time; as computing becomes faster, they should be increasingly attractive. In a slightly different vein, two-dimensional FT data processing has recently been demonstrated as an interesting approach to sorting out reaction pathways (58).

Trapped-Ion Cells

The ICR cell is the region where cyclotron excitation and acquisition of the transient takes place. The ions may also be produced within the cell or external to the cell. FT-ICR mass spectrometers use a cell in which the combination of electrostatic trapping and magnetic trapping confines the ions for a period of milliseconds to seconds. The ions ultimately leave the cell either by collisional diffusion, requiring hundreds

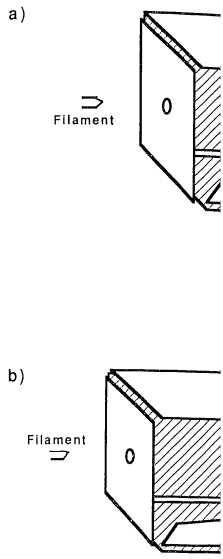

Figure 2.9 Trapped-ic
cylindrical; and (*d*) hy
serve identical functio
Spectrospin AG (*c*) and

or thousands of ion
pulse that purges t
The trapped-ion
arranged surfaces. T
ions in a region wh
excitation voltages,
these functions is u
ping is accomplish
dicular to the magn
can be carried out
use separate pairs
amplifiers, which r
preamplifier. Figur
appeared in the lit
Cell dimensions
ic field. A large cell
without space-charg
the extreme, peak s
will hold approxim
ions that can be det
will increase the d
along the z axis (a r

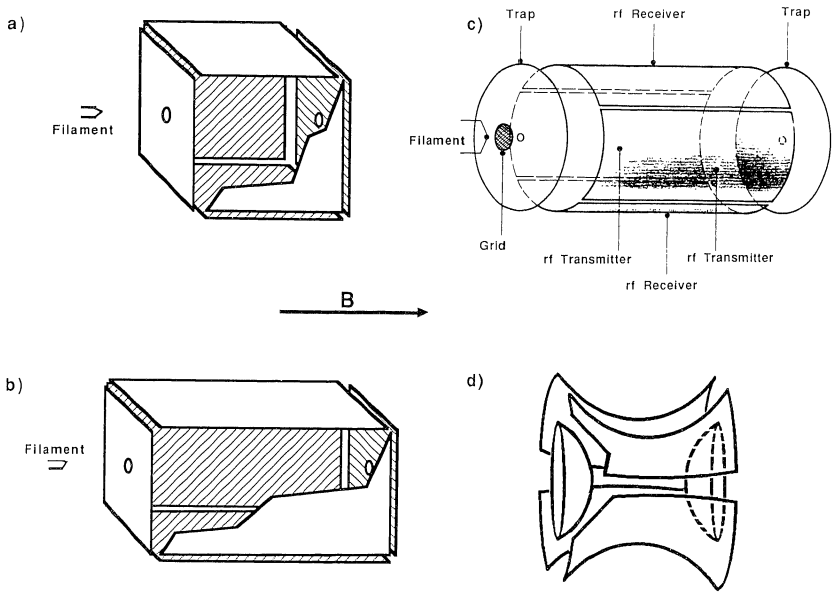

Figure 2.9 Trapped-ion cell geometries; (*a*) cubic; (*b*) orthorhombic (rectangular); (*c*) cylindrical; and (*d*) hyperbolic. Plate functions are labeled in *c*. Corresponding plates serve identical functions in the other cell geometries. [Figures supplied courtesy of Spectrospin AG (*c*) and A. G. Marshall (*d*)].

or thousands of ion-neutral collisions, or by a reverse-polarity quench pulse that purges the cell.

The trapped-ion cell is typically composed of six orthorhombically arranged surfaces. The cell accomplishes three purposes. It confines the ions in a region where excitation and detection takes place, applies the excitation voltages, and receives the induced detection current. Each of these functions is usually carried out by a set of opposite plates. Trapping is accomplished by applying potentials to the two plates perpendicular to the magnetic field lines. Although excitation and detection can be carried out on the same pair of plates, in practice it is easier to use separate pairs of plates. This simplifies isolation of the excitation amplifiers, which may transmit greater than 100 V, from the detection preamplifier. Figure 2.9 illustrates several cell geometries that have appeared in the literature.

Cell dimensions are limited by the size of the homogeneous magnetic field. A large cell volume is desirable because more ions can be held without space-charge effects, which cause ion frequency shifts and, in the extreme, peak shape distortion. A typical cubic cell (Figure 2.9*a*) will hold approximately 10^6 ions. Because the minimum number of ions that can be detected remains essentially the same, a larger volume will increase the dynamic range of the cell. In particular, elongation along the z axis (a rectangular cell, Figure 2.9*b*) takes advantage of the

homogeneous field volume of a superconducting magnet (59). Larger separation between the detection plates (x or y axis) has the advantage of increasing the amount of ion kinetic energy possible before ejection for MS/MS experiments. Cylindrical cells as used by Spectrospin (Figure 2.9c) also make more efficient use of the available homogeneous field volume.

The most important function of the cell is to provide an environment where extremely accurate mass and resolution measurements can be made. Current commercial cells accomplish this goal to the extent that these capabilities are comparable to or better than those of the best traditional mass analyzers. Although excellent, these capabilities can be further improved, largely by removing or accounting for nonideal ion behavior. This is an area of active research, and a consensus has not been reached on the optimum cell design. The remainder of this section will discuss sources of nonideal behavior and some proposed solutions through cell geometry and additional cell elements.

Undesirable Effects due to Nonideality of the Electric Field

Electric Field Shapes

The static electric field for ion trapping in the ideal ICR cell would have all the trapping field lines directed along the z direction (magnetic field direction) and pointing inward toward the z = 0 plane. However, Laplace's law only permits this along the z axis, and everywhere else in the cell the trapping field has radial components pointing toward the excite and detect plates. Similarly, ideal rf electric fields used for excitation would be perpendicular to the excitation plates, but the presence of the trapping plates leads to components of the rf field parallel to the z axis. The ion motions are complicated by these nonideal field components. The types of nonideal behavior can be summarized as (1) ion frequency dependence on trapping voltage, (2) ion frequency dependence on position, (3) radial high-mass ejection, and (4) excitation and ejection along the z axis during the rf excitation. Several approaches to alleviating these effects by clever geometries and field-shaping hardware are discussed in the following sections.

Frequency Dependence on Trapping Potential and Ion Position

In an ideal cell, the ion frequency would be independent of both trapping potential and ion location within the cell. The radial component of the trapping field leads to a deviation from this ideal, producing a downward shift in frequency that is proportional to the trapping volt-

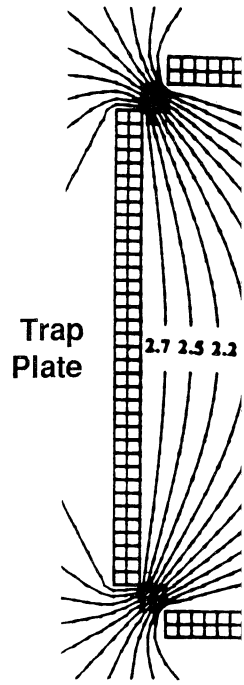

Figure 2.10 A diagram c
in a cubic cell. An ion
toward the center of the
that has both an axial c
figure supplied courtesy

age. Figure 2.10 qu
gins of the radial co
of the cell (ion a) wi
z axis. An ion off a
has both an axial
force due to the m
seen that the radial
force. This results i

Upper Mass Limit

The radial electrost
the upper mass tha
when the outward r
er than the inward

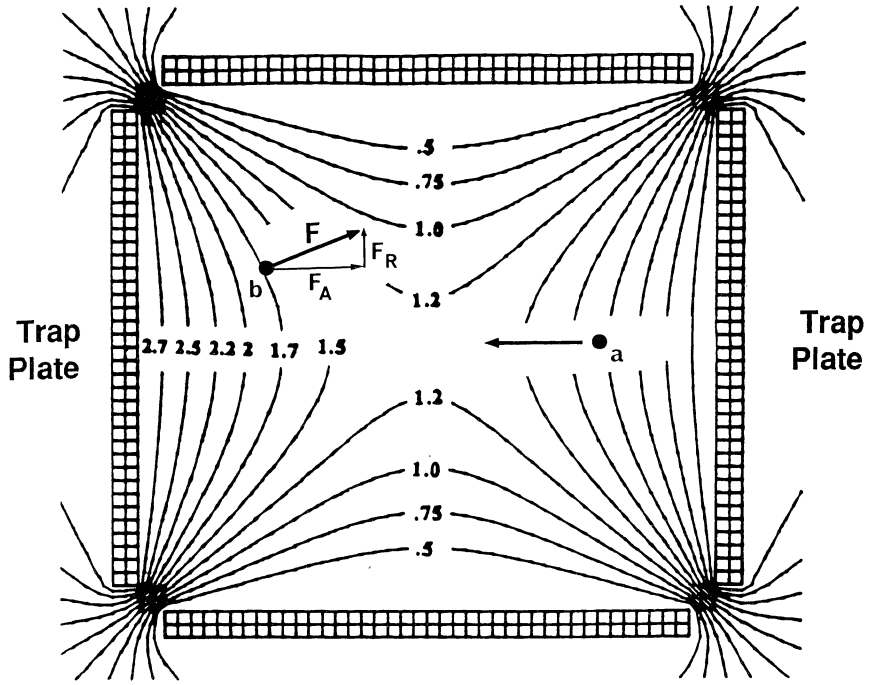

Figure 2.10 A diagram of equipotential electric field lines due to a 3-V trapping potential in a cubic cell. An ion along the cell axis (ion a) is subjected to a force directed only toward the center of the cell. An ion off the central axis (ion b) is subjected to a force $\boldsymbol{F}$ that has both an axial component ($\boldsymbol{F}_A$) and a radial component ($\boldsymbol{F}_R$). (Modified from a figure supplied courtesy of D. H. Russell.)

age. Figure 2.10 qualitatively illustrates the electric field and the origins of the radial component for a cubic cell. An ion on the central axis of the cell (ion a) will be acted on by an electric field directed along the z axis. An ion off axis (ion b) will be acted on by an electric field that has both an axial and radial component. Recalling that the Lorentz force due to the magnetic field is directed radially inward, it can be seen that the radial electric field component acts against the Lorentz force. This results in a decrease in the ions' cyclotron frequency.

Upper Mass Limit

The radial electrostatic component of the trapping potential also limits the upper mass that a cell can trap. The upper mass limit is reached when the outward radial component of the trapping potential is stronger than the inward directed Lorentz force. The upper mass limit can be

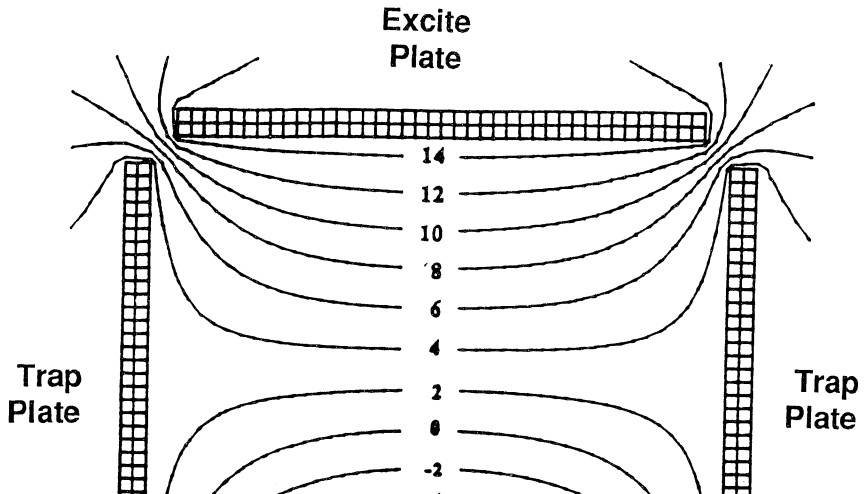

Figure 2.11 A diagram of equipotential electric field lines due to rf excitation. At this instantaneous time, the top plate is at + 15 V and the bottom plate at − 15 V. An ion not along the central vertical axis will be subjected to a force directed either inwards or outwards (depending on the local electric field gradient). (Figure supplied courtesy of D. H. Russell and used with permission from Ref. 64.)

increased by increasing the magnetic field strength or decreasing the trapping voltage. This effect is discussed further under Performance.

Z-Axis Excitation

During excitation, an rf field is applied to a pair of plates perpendicular to the trapping plates. Analogous to the trapping case, bending of the rf field lines toward the nearby trapping plates creates a field component along the z axis (Figure 2.11). This high-frequency component may lead to a resonant oscillation of the ion along the z axis. It has been shown by Kofel et al. (45) that during chirp excitation the ion will absorb energy through this process at frequencies slightly above the ion cyclotron frequency and may be ejected along the z axis.

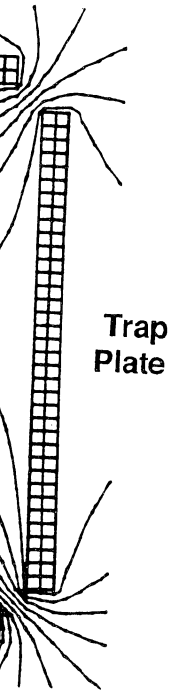

citation. At this
15 V. An ion not
ther inwards or
d courtesy of D.

creasing the
rformance.

rpendicular
ding of the rf
component
nt may lead
been shown
will absorb
ve the ion

Field-Corrected Cells

Field Corrections through Cell Geometry

Several trapped-ion cell geometries have been reported that were constructed to reduce the effects of the radial component of the trapping potential. Elongated cells of rectangular (59) (Figure 2.9*b*) and cylindrical (60) (Figure 2.9*c*) design have been used with some success to reduce the effect of the trapping potential on ion frequencies since the radial trapping-field component is reduced in the central region where the ions are trapped.

The hyperbolic cell geometry as proposed by Wang and Marshall (61) (Figure 2.9*d*) has the particular property that the radial field component and, hence, the frequency shift is the same at all positions in the cell. This cell still suffers from a cyclotron frequency dependence on trapping potential. In addition, the hyperbolic cell is hard to construct and also makes very inefficient use of the magnet volume. All other cell geometries have the added problem that the frequency shift due to the trapping field varies with ion position, which lowers mass resolution when the ion cloud has finite dimensions.

Field Correction by Auxiliary Electric Elements

Several hardware modifications have been proposed that promise to improve cell behavior. Four recent designs are shown in Figure 2.12. These cells are all designed to reduce nonperpendicular components of either or both the trapping and excitation electric fields.

Wang and Marshall have developed the screened cell (62) (Figure 2.12*a*), which greatly reduces the dependence of ion frequencies on the trapping potential and also eliminates high-mass ejection by the radial trap potential. The objective of this design is to reduce the trapping potential to near zero over most of the cell volume and trap the ions by strong, but localized repulsive fields near the trapping plates. Grounded screens are used to shield the volume of the cell from the trapping fields. This design reduces the trapping potential by a factor greater than 10 just inside the screen. In an orthorhombic cell, the use of grounded screens was shown to reduce the frequency dependence on trapping potential by a factor of 100. In addition, mass calibration accuracy improved, because the magnitude of the correction for trapping potential in the calibration equation decreased.

As pointed out by Marshall, the resolution of both excitation and detection increases because the ion frequency is independent of its location within the cell. The improvement in excitation resolution in tandem with SWIFT excitation should be especially significant. In nonscreened, nonhyperbolic cells, high-resolution ion excitation and ejection is limited because the cyclotron frequency of an ion changes as its

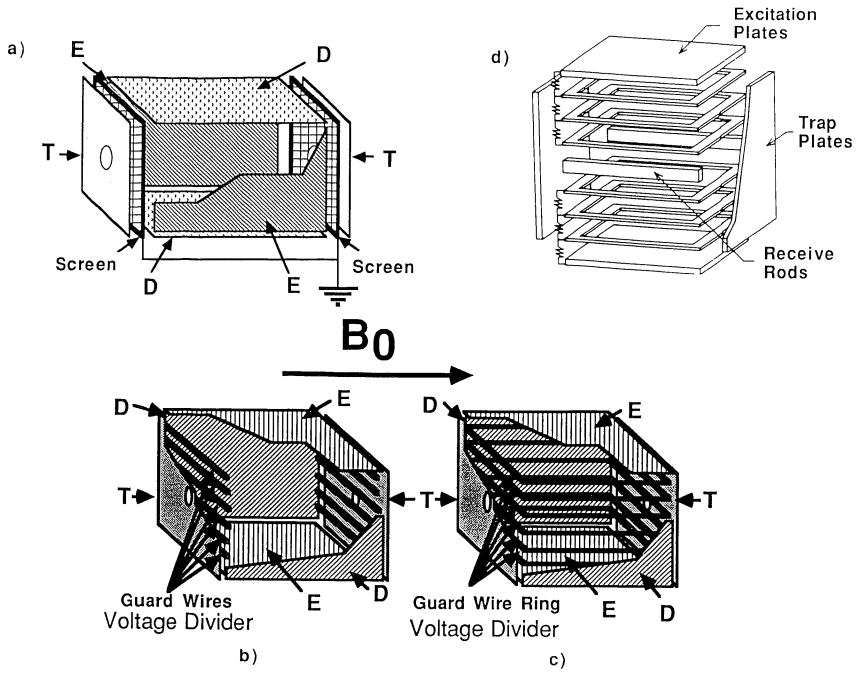

Figure 2.12 Field-corrected cells: (*a*) screened orthorhombic cell, (*b*) rf-shimmed cell with guard wires, (*c*) rf-shimmed cell with guard rings, (*d*) rf-shimmed cell with guard rings and detection rod. [Figures supplied courtesy of A. G. Marshall (*a-c*) and D. H. Russell (*d*) and used with permission from Ref. 62 (*a*), Ref. 63 (*b* and *c*), and Ref. 64 (*d*)].

orbital diameter increases. In a screened cell, the cyclotron frequency stays the same regardless of ion radius. High-resolution excitation is particularly useful for mass selection in MS/MS experiments.

The use of voltage divider circuitry for rf shimming has independently been reintroduced by Wang and Marshall (63) and Russell and co-workers (64) [voltage dividers were used for rf shimming on the original omegatron over 40 years ago (65)]. In Wang and Marshall's designs, guard wires (Figure 2.12*b*) or guard rings (Figure 2.12*c*) are placed within the cell. In the guard wire version, a set of wires is placed in front of each trap plate. The wires are part of a voltage divider circuit, which progressively lowers the rf voltage applied to the wires away from the excite electrode. In the guard ring version, ring electrodes (again part of a voltage divider circuit) are placed in the cell shielding both the trap and detect plates. In both designs the purpose of the shimming electrodes is to produce a uniform rf field in the volume within the electrodes. This means that (1) even excitation is applied to ions regardless of initial location, leading to better quantitation, (2) z excitation and ejection is eliminated, and (3) shielding of the volume from the trapping potential reduces the dependence of frequency on

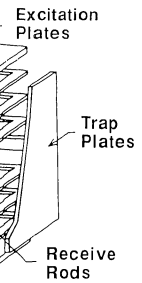

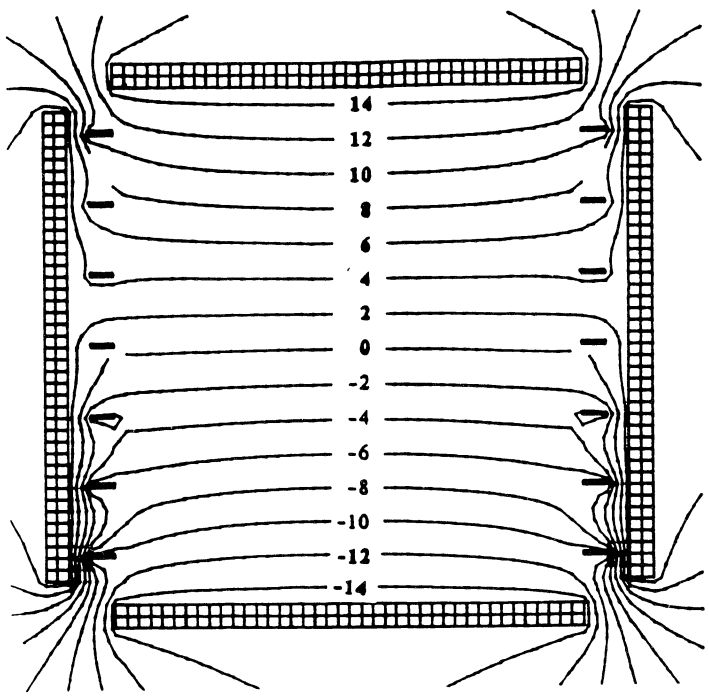

Figure 2.13 Equipotential field lines in the rf-shimmed cell designed by Russell's group (cell *d* of Figure 2.12) with ± 15V applied to the excite plates. Compare with field lines in nonshimmed equivalent cell in Figure 2.11. (Figure supplied courtesy of D. H. Russell and used with permission from Ref. 64.)

trapping potential, although not as well as the screened cell. A disadvantage is that signal is reduced through partial screening of the detection plates and unavoidable loss of trapping efficiency. Wang and Marshall have suggested two solutions involving the switching of the ring electrode circuitry to eliminate the screening of the detection electrode.

In the design of Hanson et al. (64) (Figure 2.12*d*,) a rod electrode replaces the plate electrode for ion detection. The sensitivity of the receiver rod was measured to be as good as or better than a receiver plate at all ion excitation radii except close to ion ejection. The equipotential field lines during excitation are shown for the cell in Figure 2.13. A comparison of this figure with Figure 2.11 clearly shows that the undesirable radial component of the electric field is reduced throughout the volume of the cell.

Though field-corrected cells have not been fully evaluated, it appears that the use of these cells will allow another incremental im-

provement in the already excellent mass accuracy of FT-ICR. We can hope that some of these design features will be incorporated in the next generation of commercial instruments.

Magnets

Superconducting magnets have been preferred for FT-ICR because of their extremely stable magnetic field and the high field strengths possible. High magnetic fields are desirable because resolution, the signal-to-noise ratio, and the upper mass limit (as determined by the radial component of the trapping potential) all increase with magnetic field strength. The resolution increases linearly with field strength under most conditions of peak broadening. Signal-to-noise ratios are also expected to increase with the square root of the field strength. While this improvement in signal-to-noise ratios is not as dramatic as seen in NMR, which goes approximately as the 7/4 power of the field strength, it still is significant. Under conditions where the upper mass limit is determined by the radial trapping field (described under Mass Range), the higher field strength also raises the high-mass limit of the instrument linearly.

As described in the Chapter 1, the superconducting solenoid produces an elongated homogeneous magnetic field region. This geometry allows extremely long, high-capacity cells. The elongated field region also facilitates suspended-trapping operating sequences (described in Chapter 3), which are reported to improve mass accuracy. The cross-sectional homogeneous field region is also larger than that of an electromagnet, allowing 2-in. or larger cubic cells, whereas 1-in. cells are typical in electromagnet-based instruments.

A relatively minor drawback of using higher fields is that the lower mass limit may be restricted by the A/D converter bandwidth. For example, the FTMS-2000, once offered by Nicolet, has a 2.667-MHz A/D converter, which leads to a lower mass limit of 17 Da at 3 T. Masses lower than 17 Da have frequencies that are greater than 2.667 MHz, so that the Nyquist requirement is not fulfilled and these masses will appear in the spectrum as folded-back or aliased peaks. The practical mass limit is actually lower, because these aliased peaks can usually be identified by their unusual nonintegral masses. This is not a serious limitation because the actual mass of a foldover peak can easily be calculated. Nicolet's software includes a software command to calculate foldover masses (66).

The accessibility of the trapped-ion cell is more restricted with the superconducting magnet than with the electromagnet geometry. Probes, pulsed valves, lasers (for desorption, photodissociation, or multiphoton ionization), optical viewing equipment, and so on must be introduced along the cell axis parallel to the magnetic field. A charged

beam, such as the electron beam or an ion beam from an external source must also be aligned along this axis. Except for charged-particle beams, external hardware and beams can be introduced radially in an electromagnet geometry. For these reasons, an electromagnet may be more appropriate in specialized nonanalytical applications.

Differentially Pumped Configurations

Sample introduction methods, such as GC and LC, and ionization methods, such as FAB and SIMS, all impose a heavy gas load on the vacuum system and with typical interfacing are incompatible with high-resolution FT-ICR MS measurements. An ingenious approach to this problem, the dual cell, was developed by EXTREL FTMS. An alternative, the external ion source, has been developed commercially by Spectrospin and IonSpec and also has been developed independently by several researchers. External ion source instruments use ion transfer techniques to move the ions into the ICR cell for excitation and detection. These approaches are discussed below.

Dual Cell

In the commercial configuration, the dual cell (67,68) consists of two cubic cells sharing a common center trap plate (Figure 2.14). The shared trap plate forms a barrier between the two cell regions; the only gas communication between the two differentially pumped sides of this plate is through a small hole termed the *conductance limit* on the cell's central axis. Each cell has its own rf transmitting and receiving connections, allowing either cell to be selected under computer control. The pressure differential achieved depends on the size of the conductance limit. In the commercial instrument, the 2-mm-diameter conductance limit will give a pressure differential of 1000:1.

An example of the use of the cell for GC is shown in Figure 2.15 (69). The GC effluent enters the *source cell* and is ionized by an electron beam passing through both cells. During the ionization pulse, the center trapping plate is at zero potential, and ions are free to pass between the two cells. Motion in the x–y plane, which would move ions off axis to the conductance limit, is not possible due to the magnetic field. Because the electron beam time is long relative to the ion oscillation between cells, the ion populations equilibrate between the cells. After the ionization period, the conductance limit is "closed" by applying a voltage equal to the trapping potential. Excitation and detection is then carried out in the low-pressure *analyzer cell*.

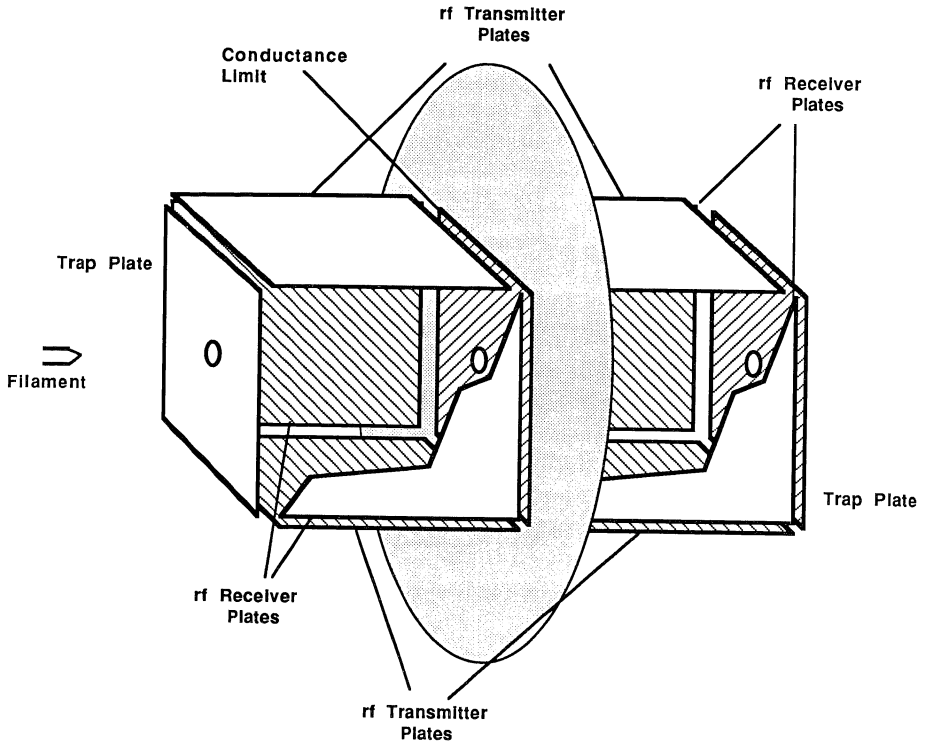

Figure 2.14 A diagram of the Nicolet dual trapped-ion cell. The *conductance limit*, or center trap plate, is incorporated in the wall separating the two differentially pumped regions.

External Ion Sources

The historical evolution of the external ion source of ICR is well described in Chapter 9. At this point, we will summarize several external source designs in current use. More detailed descriptions of specific instruments are available in later chapters by external source users. External ion source instruments all use several stages (typically three) of differential pumping to reduce the pressure in the ICR cell. The major difference between external ion source designs is the method of guiding the ions into the ICR cell.

Spectrospin has developed an external ion source that uses a series of electrostatic lenses to guide the ions into the ICR cell (70). The ions are accelerated to several thousand electron volts, focused, and decelerated just outside the ICR cell (Figure 2.16). The acceleration of the ions increases the transmission efficiency through the fringing magnetic field. The ion source, transfer region, and ICR cell are all differentially pumped. This configuration gives a pressure differential of 10^4 (70) between the ion source and the ICR cell. An early version of this

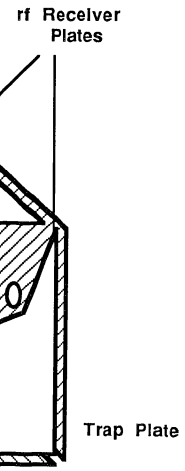

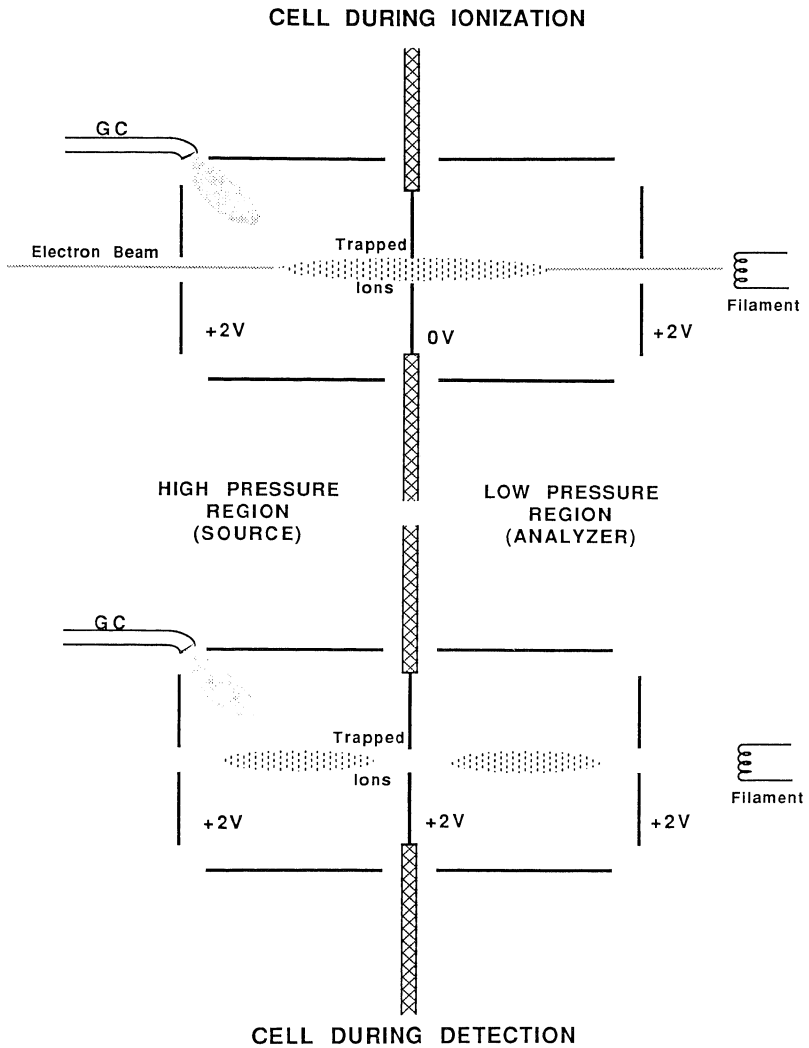

Figure 2.15 The operation of a dual cell in the GC EI mode. The diagram shows a cross section of the source (high-pressure) and analyzer (low-pressure) cells. During ionization (*top*), the electron beam is on, and ions are formed in the region between the end trap plates. The electron beam duration (~5 ms) is long compared to ion motion between the two cells; therefore ions formed in either cell equilibrate between the two cells. During the detection period (*bottom*) the center plate is "closed," and the two ion populations are isolated. The population of the ions in the low-pressure cell is detected.

source/lens system suffered from a low-duty cycle, because, although ions are produced continuously in the external source, only the portion formed during the pulsing of ions into the cell are actually analyzed. The current commercial version features a patented method (71) to continuously accumulate ions within the cell. This results in improved

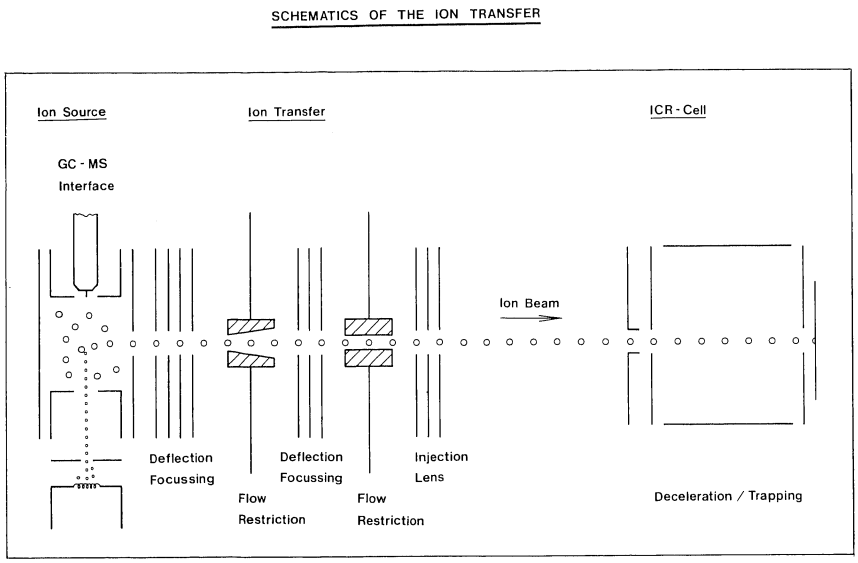

Figure 2.16 A diagram of ion optics used by the Spectrospin external ion source for transferring externally created ions to the ICR cell. (Courtesy of Spectrospin AG.)

sensitivity. Chapter 4 presents a more detailed description of this design.

The American Cyanamid instrument, described in Chapter 9, also uses lenses to guide ions through the fringing field of the magnet. In addition, rf quadrupoles are used to prefilter and focus the ions emerging from the external ion source. Three differentially pumped regions are present in the vacuum system. Each region can be isolated and is cryogenically pumped.

McIver et al. (72) have designed an instrument, marketed by IonSpec, that uses long quadrupole rods to guide ions from an external source to the ICR cell (Figure 1.7). The ions are not accelerated through the fringing fields because sufficient guidance is provided by the quadrupole rods. This arrangement has the additional advantage of preselecting ions for passage to the ICR cell. In this way, solvent, background, or other undesirable ions can be excluded from the cell, improving the detection limits and dynamic range of the analysis. A prototype for this instrument is described in Chapter 8.

Performance Factors

The performance of a mass analyzer is evaluated in terms of resolution, mass accuracy, sensitivity and dynamic range, and mass range. In addition, the versatility of the analyzer should be considered (e.g., ease of switching between positive and negative ion detection, speed of analysis, source accessibility, and software control). FT-ICR MS excels in

resolution and mass accuracy. Resolving power (*RP*) of over 1 million is routinely achieved in the heterodyne mode, and tens of thousands (often limited by computer memory) is easily achieved in full-spectrum mode. Mass accuracy is as good as or better than high-resolution magnetic sector instruments. In addition, the mass measurement stability is extremely good. The dynamic range of an FT-ICR MS is not as high as some other analyzers, largely due to the limitation in the number of ions that can be trapped in the cell. Hardware and techniques are actively being developed (such as SWIFT and suspended trapping) that will improve all aspects of performance. This section will discuss these factors, considering the best achievable performance, the performance in routine analyses, and in comparison with the capability of other analyzer types.

Resolution

Resolution is the ability to separate two adjacent masses. The definition that will be used is

$$R = 1/RP = \delta m_{\text{half height}}/m \qquad (2.4)$$

where R is the resolution, RP is resolving power, m is the measurement mass, and $\delta m_{\text{half height}}$ is the peak width at half-height. This definition will just resolve a peak at mass m from a peak at mass $m + \delta m$. (Note that resolving power is often informally referred to as the *resolution*.) In FT-ICR MS, resolving power is inversely proportional to mass. In other words, if the RP is 10 000 at mass 50, then RP will be 1000 at m/z 500. Quadrupole analyzers operate in a constant δm mode (tuning for an RP of 50 at m/z 50 will give an RP of 500 at m/z 500), and magnetic sector analyzers operate at constant $m/\delta m$ (RP of 1000 at m/z 50 will result in an RP of 1000 at m/z 500). Although the FT-ICR MS dependence of resolution on mass is less favorable for high-mass analyses than quadrupole and magnetic sector instruments, for routine operation in typical mass ranges FT-ICR MS is as good as or better than high-resolution magnetic sector analyzers and at least an order of magnitude better than quadrupole analyzers. In heterodyne mode, FT-ICR MS routinely achieves resolving power of 1×10^6 at m/z 131 at 3 T.

For magnetic sector analyzers, sensitivity must be sacrificed to achieve resolution. (At a resolving power of tens of thousands, only a fraction of a percent of the ions will be transmitted from the source to the detector in a magnetic sector instrument.) For FT-ICR MS, in some cases sensitivity actually improves with resolution. The precision of the mass measurement, and thus the resolution, is a reflection of the amount of time the coherent cyclotron motion of a packet of ions can be observed. The dependence on observation time is a result of the need to measure the ion frequency accurately. The observation time is limited by the decay of the ICR signal transient in the time domain, correspond-

ing to peak broadening in the frequency domain. Recalling that immediately after excitation, packets of ions of the same mass are moving in circular orbits, the decay of the transient results from the spreading of these packets by inhomogeneous electric and magnetic fields and from the scattering of ions out of the packets by collisions with neutral molecules. With superconducting magnets, field homogeneity is usually not a limiting factor except for the special cases of large or elongated cells. Usually, collisional broadening is the predominant cause of transient signal decay, so the maximum observation time is limited by the pressure. A rough estimate of the duration of the signal is given by Comisarow (73):

$$\text{duration (s)} = 2 \times 10^{-8}/\text{pressure (torr)} \qquad (2.5)$$

At 2×10^{-8} torr, the ions can be observed approximately 1 s.

In some cases, acquisition parameters may be set such that the entire transient is not observed. The resolution can then be doubled by doubling the acquisition time to include more of the transient. This will also improve the signal-to-noise ratio. Because the easiest way to increase the acquisition time is by acquiring more samples, the limiting factor becomes the data system. Typically, 128 K to 256 K are the maximum number of samples that a data system can handle. Another way to increase the observation time is to increase the sample interval. Again if the sampling interval is doubled (i.e., the sampling rate is halved), the acquisition time will be doubled. The limitation of this strategy is that the sampling rate must remain twice the value of the highest frequency observed or else the frequency will be undersampled. A third way to increase observation time is to use the heterodyne detection mode, gaining high resolution at the cost of limiting the range of masses observed.

The magnetic field strength plays a major role in resolution and sensitivity. For given sampling conditions and data acquisition parameters, the resolution can be improved by using a higher magnetic field. Resolution increases linearly with field strength, as shown by equation 2.6 (74).

$$m/\delta m = q\boldsymbol{B}\,\tau/2m \qquad (2.6)$$

In this equation, q is the electron charge, $\boldsymbol{B}$ is the magnetic field strength, and τ is a signal decay constant. The inverse relation of resolution on mass is also shown in this equation. Some of the best resolutions reported in the literature for low mass, working mass, and high mass are listed in Table 2.2.

Mass Accuracy

Although most specifications emphasize mass resolution in FT-ICR MS, it is mass accuracy that is required by many applications. In the BP

Table 2.2 Examples of High Resolution by FT-ICR MS

Field (T)	Resolution	Mass	Compound	Reference
7.02	2×10^8	40	Argon, 90 s transient	75
4.7	1.1×10^7	131	PFTBA	76
4.7	3×10^5	1466	(Perfluorononyl)-*s*-triazine	76
7	1.6×10^5	3200	PEG-3350	77
7	5×10^4	5922	PPG-4000	77
7	53 000	9746	$(CsI)_nCs$	78

Abbreviations: FT-ICR MS, Fourier transform ion cyclotron resonance; PFTBA, Perfluorotributylamine; PEG, Polyethylene glycol; PPG, Polypropylene glycol

laboratory, a mass accuracy of 5 ppm is typically achieved at m/z 500 (79); Stockton et al. routinely obtain a mass accuracy of 1 ppm (see Chapter 9). Accurate mass measurement allows molecular formula determinations because most elements do not have integral molecular weights. For example, $[C_2F_4]^+$, $[C_6H_{12}O]^+$, and $[C_7H_{16}]^+$ have exact masses of 99.9931, 100.0883, and 100.1247 Da, respectively (including an allowance for the loss of an electron), so they can be distinguished if the ionic mass is measured with sufficient accuracy.

Mass accuracy is often reported in parts per million.

$$\text{mass accuracy (ppm)} = (m_{\text{actual}} - m_{\text{measured}})/m_{\text{ave}} \times 10^6 \quad (2.7)$$

Therefore, an accuracy of 952 ppm is needed to distinguish $[C_2F_4]^+$ and $[C_6H_{12}O]^+$. The number of possible molecular formulas and, hence, the required mass accuracy increases exponentially with mass. A mass accuracy of 5 ppm at 500 Da is practically useful, especially if some limits can be placed on elemental composition. For unambiguous elemental composition, a mass accuracy of better than 1 ppm may be needed. A detailed example illustrating this point is presented in Chapter 9.

Mass accuracy depends to some degree on resolution and signal-to-noise ratios. Insufficient resolution will degrade accurate mass measurement when two peaks are not totally resolved. This will shift the apparent mass of both peaks toward each other. If interfering peaks are not present, the peak position can be determined by FT-ICR MS to an accuracy that is a small fraction of its width. In this case, mass accuracy in FT-ICR MS is more affected by electric field inhomogeneities caused largely by trapping voltages and space–charge interactions. Active research in understanding these effects that lead to small perturbations to the ion cyclotron frequencies is resulting in improved mass accuracy through hardware developments (discussed under Trapped-Ion Cells) and calibration methods. Other possible sources of error, such as magnetic field inhomogeneity (80) and magnetic field drift (81), have been determined to be insignificant with superconducting magnets.

The basic cyclotron equation provides the simplest calibration equation for the mass of an ion in the absence of electric fields:

$$m/e = \boldsymbol{B}/2\pi f \tag{2.8}$$

or replacing constant terms with a

$$m/e = a/f \tag{2.9}$$

where m is the mass, e is the electron charge, f is the cyclotron frequency, and $\boldsymbol{B}$ is the magnetic field value. The mass is simply inversely proportional to f. In fact, electric fields do exist in the cell due to the trapping plate voltages and the space charge of the ions themselves. The effect of the radial trapping electric field component on mass has been approximated by Ledford et al. (82) as

$$\delta m/e = -2G_T V_{eff}/(4\pi^2 f^2) \tag{2.10}$$

where G_T is a geometry factor for the cell defined by Jeffries et al. (83) and V_{eff} is the effective trapping potential. Replacing the constant terms with b and adding to equation 2.9 gives

$$m/e = a/f + b/f^2 \tag{2.11}$$

Equation 2.11 is the most frequently used calibration equation. In practice, a series of known mass/frequency pairs are fitted to the equation, and the constants a and b are determined. This calibration is then applied to unknown frequencies in the spectrum.

The effect of ion space charge is qualitatively equivalent to the effect of the trapping potential (Figure 2.17). An ion cloud has a radial electric field component that opposes the magnetic field. Because the form of the space-charge electric field is similar to the trapping potential, calibration effects introduced by the space charge are also accounted for in the second term of equation 2.11. This then introduces the requirement that the number of ions in the cell during the calibration is approximately the same as the number of ions for the sample measurement. Experimental measurements on a 1.9-T system with a 0.0254-m cubic cell gave a shift of −9.75 Hz per 10 000 ions (82). One should note that calibration shifts due to trapping potential or space charge are linear with frequency. Because mass is inversely proportional to frequency, the absolute mass error is larger at higher mass.

Suspended Trapping Sequences

Laude and co-workers (84–86) have developed a pulse sequence, described in Chapter 3, to alleviate space charge effects within the trapped ion cell. This procedure has two major advantages: It improves peak shapes at high densities, and more pertinent to this section, it levels out the number of ions within the cell, regardless of how many ions are initially formed. This is especially significant in laser desorp-

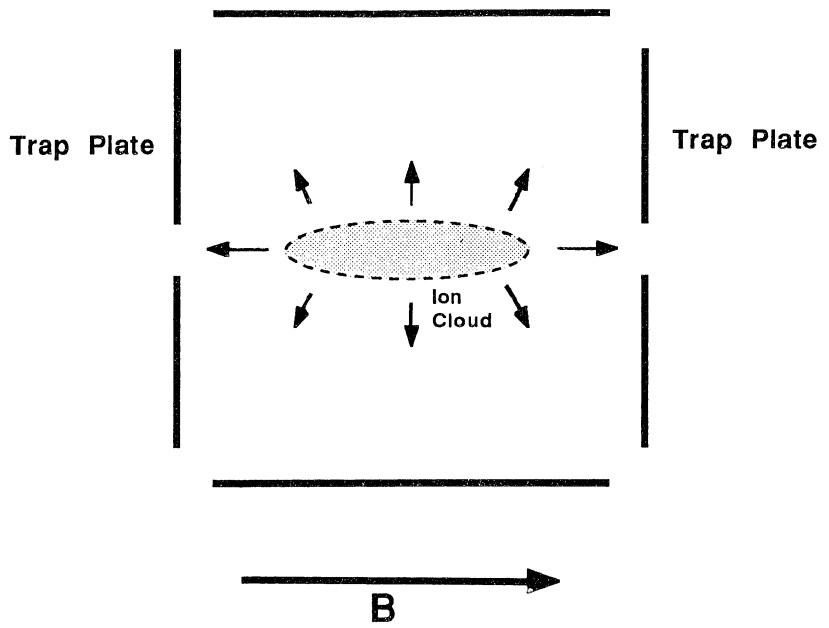

Figure 2.17 A qualitative view of the electric field associated with ion space charge. The radial component of this field has the same effect as the radial component of the trapping electric field.

tion-ionization and GC/MS, where the number of initially formed ions can vary over several orders of magnitude. The modification to the ICR pulse sequence is trivial; after ion formation, the trap plate potentials are dropped to zero for a period of microseconds, allowing a portion of the ions to leave the cell. This effect is self-regulating; larger initial ion populations will lead to greater ion loss from the cell. In GC/MS, Hogan and Laude (86) noted a frequency shift of less than 3 Hz (10 ppm at m/z 141) over a range of five orders of magnitude concentration of methylnaphthalene injected onto the GC column (3-T superconducting magnet).

Other Sources of Mass Calibration Error

The derivation of the two-parameter calibration equation described above neglected the effect of collisional damping on the frequency, which is valid at pressures less than 10^{-6} torr. Other approximations are made as to the nature of the radial component of the electric field and the ion–ion interactions. The frequency shift due to the radial electric field is assumed to be constant anywhere within the cell, which is only true for hyperbolic cells and fully screened cells. Some methods of reducing the radial electrostatic fields have been investigated by several groups and are discussed in the section on trapped-ion cells.

Another source of error arises because ions of different masses do not necessarily experience the same space charge. A calibration equation, assuming that ions of a single mass only feel the electric field due to different masses, has been derived by Smith (87).

Sensitivity and Signal-to-Noise Ratios

MS, among the molecular spectroscopies (IR, NMR, and UV) is noted for its high sensitivity. In cases where extremely limited sample is available (e.g., biological samples, trace contaminants, and small inclusions), MS is the method of choice. Sensitivity can be considered at two levels. The overall sensitivity depends on the performance of the entire system. In a more fundamental sense, sensitivity is determined by the minimum number of ions necessary to produce a usable signal. This puts a premium on maximizing the signal-to-noise ratio for weak signals.

The efficiencies of sample introduction, ionization, ion accumulation or transmission, and detection will all affect the overall sensitivity. Although sensitivity is always specified in vendor performance literature, the variation in measurement conditions makes it difficult to compare instruments from different vendors. Quadrupole and magnetic sector manufacturers specifications generally vary from 50 to 500 pg sensitivity for methyl stearate introduced by GC/MS with signal-to-noise ratios of 10:1 to 200:1 in a full scan mode. Single-ion monitoring can improve this by more than a factor of 10. The quadrupole ion trap is generally considered an order of magnitude more sensitive than quadrupole and magnetic sector instruments. These analyzers are all compatible with electron multipliers, which are capable of single-ion detection, and this is reflected in the high overall sensitivities for these instruments. With current detection systems in FT-ICR, the minimum number of ions that can be detected is approximately 100 (as described below), however, it should be noted that there are no transmission losses between the ion source and the detector as in quadrupole and magnetic sector instruments. Losses are especially large when doing high-resolution measurements in double-focusing magnetic sector instruments. Thus, the sensitivity of FT-ICR MS is comparable to other mass analyzers. For example, Spectrospin's CMS 47X is specified at 50 pg sensitivity for naphthalene injected on the GC with a signal-to-noise ratio of 10:1.

An estimate of the more fundamental sensitivity of FT-ICR MS can be derived from the *rotating monopole* view of cyclotron detection, which describes the signal as an oscillation of charge between the two detector plates of the cell. Taking this point of view, Comisarow discussed sensitivity and signal-to-noise considerations clearly and in some depth (40).

It is often estimated that under ordinary operating conditions it takes

of the order of 100 ions to give a signal above noise. We can easily derive this estimate from a rough calculation. One hundred ions correspond to 1.6×10^{-17} C of alternating charge. Taking the angular cyclotron frequency to be 10^6 rad s^{-1}, this is a current of 1.6×10^{-11} A. The input impedance of the preamplifier (typically a capacitive impedance) would be about 10^5 Ω at this frequency, so the signal will develop an rf voltage of 1.6×10^{-6} V. A low-noise broadband preamplifier might have an equivalent input noise level of 10^{-4} V rms over the frequency band 0–1 MHz (88). If the transient is acquired for 10 ms, the detector bandwidth is 100 Hz, so because the noise goes as the square root of the bandwidth, the effective detector noise is 1×10^{-6} V. Thus, the 100-ion sample will give a signal slightly larger than the noise voltage. This is a reasonable estimate for everyday work on ions of moderate masses (100–200 Da.). One can do much better (using high field, small ions, long transients, and cooled amplifiers); single-ion detection should be feasible, but is too difficult to achieve in routine practical operation.

It is straightforward to predict the effect of various design and operating features of the instrument on signal-to-noise ratios:

Magnetic field. Increasing the magnetic field improves signal-to-noise ratio, because the rf current developed by a given ion packet is proportional to the cyclotron frequency.

Acquisition time. Increasing the length of acquired transient increases the signal-to-noise ratio by the square root of the transient length as long as the signal amplitude does not drop significantly during the duration of the transient. This is one way of signal averaging to reduce noise.

Signal averaging. Similarly, averaging n transients increases the signal-to-noise ratio by $n^{1/2}$, according to the usual square-root law for signal averaging.

Cell dimensions. Changing cell size or geometry has no effect on the signal from a given number of ions as long as the cyclotron orbit passes close to the receiver plates for fully excited ions.

Low-temperature preamplifier. Cooling the preamplifier to reduce its thermal noise has the potential for major signal-to-noise ratio benefits (potentially lowering thermal noise by a factor of about 10 by going to an effective noise temperature of 4 K). This has been done by physicists using quadrupole ion traps, but not by the FT-ICR community.

Pressure. If the peaks are broadened by either field inhomogeneities or by collisions, the signal-to-noise ratio is degraded because the effective detection bandwidth and, hence, the noise are increased. (The frequency-domain peak is spread over more spectral elements, each of which contributes noise.) Thus, maximum signal-

to-noise ratio is achieved when the peaks are no broader than the width imposed by the length of transient acquisition.

Number of ions. The number of ions in the ion packet will fluctuate, both because of fluctuation in the ionizing device and the unavoidable statistical fluctuation. Statistically, the number of ions will vary by $n^{1/2}$, where n is the number of ions. Thus, the fluctuation in signal for repetitive scans by using a sample of 1000 ions will be about 3%, plus any fluctuation introduced by the ion source.

A/D converter. The A/D converter introduces digitization noise because of its limited bit resolution and also gives peak variations and spurious peaks when extreme excursions in the transient are clipped. Thus, the A/D converter should have as many bits of resolution as is compatible with the necessary acquisition rate.

Dynamic Range

Dynamic range is closely related to sensitivity, because in some cases it is possible to simply increase the number of total ions formed to increase sensitivity. In ICR, this approach is limited by the total number of ions that can be trapped, which in turn is limited by the ICR cell dimensions. A scanning mass spectrometer may have a dynamic range of greater than 10^6. FT-ICR MS has a dynamic range of approximately 10^3 to 10^4 determined by the mininum number of detectable ions, 100, and the cell capacity, approximately 10^6.

The dynamic range can be improved by removing high-abundance ions from the cell. In an early example of an analytical application, Reents (89) measured low-level impurities in BF_3 by ejecting BF_2^+ from the cell, which accounted for 95% of the total ionization. BF_3^+, accounting for approximately 5% of the ionization, was used as a quantitative reference, and low-abundance compounds at 100 ppm were detected. SWIFT will further improve the capability of FT-ICR MS with respect to dynamic range by allowing high-resolution ejection of abundant ions (e.g., N_2^+ in the presence of CO^+) (90).

Mass Range

The lower mass detection limit will depend on a combination of the magnetic field strength and the excite and detection amplifier bandwidths. At higher magnetic fields, lower masses appear at higher frequencies. For example, helium-4 appears at approximately 11.6 MHz at 3 T and 23.2 MHz at 6 T. These frequencies are well within the capabilities of modern electronics, and this does not usually present a problem. An additional limitation may appear if the A/D converter cannot sample at the Nyquist frequency. In this case, if the excite and detect amplifiers have sufficient bandwidth, the ion will appear as an

aliased peak. In practice, these limitations are not serious; most researchers using high field magnets are not interested in low masses (i.e., in the range of 16 Da or less). The extra cost of high-frequency amplifiers and high-speed A/D converters must be weighed against the need for low-mass analysis.

FT-ICR MS has two fundamental limits on the high-mass detection. The first may seem obvious; the ion must have a sufficiently long lifetime to be detected. Other mass analyzers, such as time-of-flight or magnetic sector analyzers, operate in the microsecond time scale, whereas the FT-ICR time scale for detection is milliseconds. This usually does not present a problem, especially for larger ions, which tend to have longer lifetimes due to their increased degrees of freedom. For short-lived ions, a higher magnetic field to increase the ion frequency may improve this situation.

The other limitation arises from the radial electric field generated by the trapping plates. Ledford et al. (82) derived an expression for the critical mass m_c, beyond which the radial force from the trapping elec-

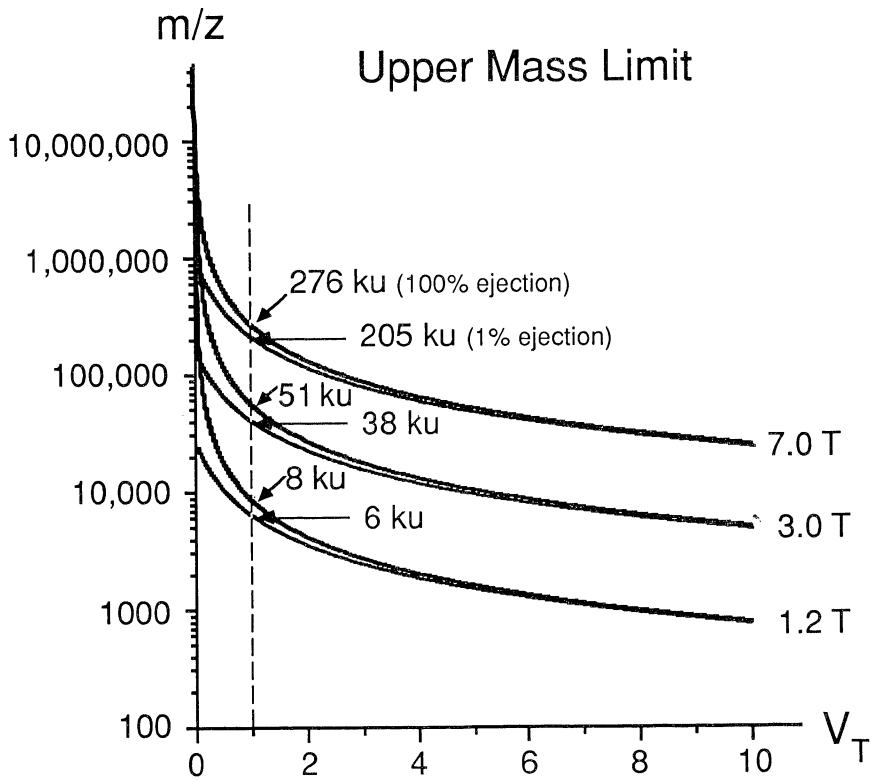

Figure 2.18 The upper mass limit as a function of magnetic field strength and trapping potential. (Figure supplied courtesy of A. G. Marshall and used with permission from Ref. 39.)

Table 2.3 Examples of High Mass Detection by FT-ICR MS

Mass	Compound	Ionization	Magnet	Reference
16 241	$Cs(CsI)_n$	Cs^+ SIMS	3	8
31 830	$Cs(CsI)_n$	Cs^+ SIMS	6	78
7 200	C_n	CO_2 laser	7	92
12 384	Cytochrome *c*	Cs^+ SIMS	7	93
29 500[a]	Carbonic anahydrase	Electrospray	3	24
66 267[a]	Bovine albumin	Electrospray	3	25

[a]Detected as multiply charged ions, actual *m*/*z* was in the range of several thousand daltons.

Abbreviations: FT-ICR MS, Fourier transform ion cyclotron resonance mass spectrometry; SIMS, secondary ion mass spectrometry.

tric field overcomes the Lorentz force and an ion initially at rest will escape radially from the cell.

$$m_c = qB^2A^2/(8\alpha V_{eff}) \qquad (2.12)$$

In this equation, q is the electron charge, $\boldsymbol{B}$ is the magnetic field, A is the cell diameter, V is the trapping potential, and α is a constant associated with the cell geometry as described by Jeffries et al. (83). Grosshans et al. (91) have plotted a more practical upper mass limit as a function of magnetic field strength and trapping voltage (Figure 2.18). This upper limit is defined as the mass at which 99% of the thermal ions will have orbital radii smaller than the cell.

It is apparent from equation 2.12 that to avoid radial high mass ejection, a high magnetic field is desirable. In addition, a higher field will increase the frequency of a given mass, increasing the signal-to-noise ratio, and allowing operation of the preamplifier at frequencies where it may be more efficient. Some examples of high-mass detection are given in Table 2.3.

Other Features

Speed

Two similar, but distinct characteristics should be noted about FT-ICR detection; it is fast and it is a pulsed event, detecting all ions present in the cell simultaneously. The distinction between simultaneous and fast-scanning mass analysis is apparent in the analysis of a GC peak. Even a complete scan in $\frac{1}{2}$ s will show a skewing of the spectrum toward high mass if the GC component is just starting to elute or a skew toward low mass if the scanning occurs on the downside of the GC peak. Pulsed operation is also advantageous for pulsed ionization techniques, such as MPI or laser desorption.

The high speed of FT-ICR detection has been exploited in recent experiments in which the dissociation process of fragmenting ions is followed directly with time resolution as fast as 2 μs. For example, the

photodissociation of styrene ions was time resolved to give dissociation rates in the range of 10^4- 10^5 s^{-1} (94).

Positive–Negative Ion Detection

Instrumental adjustment for changing from positive to negative ion detection is trivial; the polarity of the trapping potential is simply reversed. In commercial instruments, this is done through a single software command. Although software does not yet exist for alternate positive–negative ion detection, as available with other mass spectrometers, this is a natural and simple development that can be expected in the future.

Commercial Instruments

Commercial FT-ICR MS instruments are available from EXTREL FTMS (Madison, Wisc.), IonSpec (Irvine, Calif.), and Spectrospin AG (Fällanden, Switzerland). All three instruments are based on superconducting magnets. For high-mass and high-mass-accuracy measurements, the preceding material clearly shows that the higher-field magnet option is desirable. A brief description of each of these instruments follows. Some important specifications are listed in Table 2.4.

EXTREL FTMS

EXTREL FTMS, formerly a division of Nicolet Instrument Corporation, markets the basic EXTREL 2001 system and the Laser Probe mass spectrometer system. Both feature an optional dual ICR cell, described in this chapter, and a standard 3-T magnet. A 6-T and a 2-T magnet are also available. The basic 2001 has a manual probe, a batch inlet for sample introduction, and a single cell. The more elaborate versions of the mass spectrometer have an Autoprobe, a dual cell with differential pumping, and a sample visualization system so that the laser can be directed at areas of interest on a nonhomogeneous sample (5 μm spatial resolution with a Nd:YAG laser). One of the most desirable features of the EXTREL instruments is SWIFT excitation. Other options include a GC inlet and pulsed valves for pulsing reagent gas for CI or collision gas for MS/MS. Stand-alone data systems and FT-ICR electronics have also been sold.

IonSpec

IonSpec offers a series of external source instruments that use long quadrupoles to guide ions through the fringing fields of the magnet. These instruments are based on the prototype developed by McIver et al. (72) (described in Chapter 8). Ions can be produced by EI, CI, LD

Table 2.4 Specifications on Some Instruments

	EXTREL FTMS 2001	Spectrospin CMS 47X	IonSpec QFT-7X	American Cyanamid
Magnetic field (T)	2, 3, 6, 7	3, 4.7, 7	3, 4.7, 7	7
Cell type	Dual 2 in. cubic or 2 × 2 × 4″ elongated	60 × 60 mm, rf-shimmed cylindrical	2 × 2 × 3 in., elongated	1.25 × 1.25 × 3.5 in., elongated
Radio frequency amp (p-p) (V)	120	300	200	130
ADC rate	10 or 20 MHz	20 MHz	16 MHz	10 MHz
ADC resolution (bit)	12	9, 12	9, 12	12
Maximum spectrum size	1024 K	128 K	256 K	1024 K
Computer	Risc Workstation	Bruker Aspect 3000	Compaq 486/33	Motorola 68030
Array processor	64 bit, 80 MFLOPS	Bruker	32 bit, 66 MFLOPS	Mercury, 32 bit, 20 MFLOPS
Transform and display speed (s)	0.25 (64K)	15 (64 K), 30 (128 K)	3.9 (256 K)	0.8 (128 K), 1.7 (256 K)

Abbreviations: ADC, ; MFLOPS,
ADC, Analog-to-digital converter; MFLOPS, Million floating point operations per second; K, 1024

(optional), o
introduced
trolled pulse
excitation. I
searchers wh
and cells.

Spectrospi

The CMS 47
ment feature
nal source us
the ICR cell,
this cell, the
eliminate z e
ume. EI and C
and a direct
optional. Op
optional UNI
the Sun Spar

ACKNOWLEDGM
The authors w
of J. E. Campa
We would als
providing info

References

1. Ghaderi, S
"Chemical
Chem. **198**
2. Carlin, T.J.
Gases in Fo
571–574.
3. Irion, M.P.
"Multipho
Spectrome
4. Sack, T.M.;
Multiphoto
Chem. **198**
5. Castro, M.J
Fourier Tra
6. Castro, M.J
Fourier Tra
2293.

(optional), or Cs^+ SIMS (optional). Gases or volatile liquids can be introduced either through adjustable leak valves or computer-controlled pulsed valves. Their data system, the Omega/486, offers impulse excitation. IonSpec also offers their data system separately to researchers who are constructing their own specialized vacuum systems and cells.

Spectrospin AG

The CMS 47X is the basic instrument from Spectrospin. This instrument features a 4.7-T magnet with an optional 7.0-T magnet. The external source uses electrostatic lenses to guide and accumulate ions into the ICR cell, which is a 170-cm^3 cylindrical cell. The latest version of this cell, the Infinity cell, features segmented trapping plates, which eliminate z ejection and improve rf excitation throughout the cell volume. EI and CI are standard. Standard inlets are a gas/liquid batch inlet and a direct insertion probe. A GC inlet and pulsed gas valves are optional. Optional ionization methods include LD, FAB, and FD. An optional UNIX/X11/Motif based MS processing package, supported on the Sun Sparcstation and other workstations, is available.

ACKNOWLEDGMENTS

The authors would like to acknowledge the helpful suggestions and comments of J. E. Campana, G. Kruppa, A. G. Marshall, M. J. C. Smith, and C. H. Watson. We would also like to thank EXTREL FTMS, IonSpec, and Spectrospin for providing information on their latest instruments.

References

1. Ghaderi, S.; Kulkarni, P.S.; Ledford, E.B., Jr.; Wilkins, C.L.; Gross, M.L. "Chemical Ionization in Fourier Transform Mass Spectrometry", *Anal. Chem.* **1981,** *53,* 428–437.
2. Carlin, T.J.; Freiser, B.S. "Pulsed Valve Addition of Collision and Reagent Gases in Fourier Transform Mass Spectrometry", *Anal. Chem.* **1983,** *55,* 571–574.
3. Irion, M.P.; Bowers, W.D.; Hunter, R.L.; Rowland, F.S., McIver, R.T. "Multiphoton Ionization Detected by Fourier-Transform Mass Spectrometry", *Chem. Phys. Lett.* **1982,** *93,* 357–379.
4. Sack, T.M.; McCrery, D.A.; Gross, M.L. "Gas Chromatography/ Multiphoton Ionization Fourier Transform Mass Spectrometry", *Anal. Chem.* **1985,** *57,* 1290–1295.
5. Castro, M.E.; Russell, D.H. "Cesium Ion Desorption Ionization with Fourier Transform Mass Spectrometry", *Anal. Chem.* **1984,** *56,* 578–581.
6. Castro, M.E.; Russell, D.H. "Desorption Ionization of Cesium Iodide by Fourier Transform Mass Spectrometry", *Anal. Chem.* **1985,** *57,* 2290–2293.

Transform and display speed (s)	0.25 (64K)	15 (64 K), 30 (128 K)	3.9 (256 K)	0.8 (128 K), 1.7 (256 K)	20 MFLOPS

Abbreviations: ADC, : MFLOPS,
ADC, Analog-to-digital converter; MFLOPS, Million floating point operations per second; K, 1024

7. Amster, I.J.; Loo, J.A.; Furlong, J.P.; McLafferty, F.W. "Cesium Ion Desorption Ionization with Fourier Transform Mass Spectrometry", *Anal. Chem.* **1987,** *59,* 313–317.
8. Amster, I.J.; McLafferty, F.W.; Castro, M.E.; Russell, D.H.; Cody, R.B.; Ghaderi, S. "Detection of Mass 16241 Ions by Fourier-Transform Mass Spectrometry", *Anal. Chem.* **1986,** *58,* 483–485.
9. Kellerhals, H.; Allemann, M. U.S. Patent 4,563,579, **1986.**
10. Hill, N.C.; Marshall, A.G. "A Fast Neutral Beam Ion Source for FT/ICR Mass Spectrometry", Paper presented at the 38th ASMS Conference on Mass Spectrometry and Allied Topics, June 3–8, 1990, Tuscon, Ariz., poster MP 84.
11. Marshall, A.G. Private communication, February 10, 1991.
12. Weller, R.R.; Viswanadham, S.K.; Sheetz, M.A.; Giam, C.S.; Hercules, D.M. "Californium-252 Plasma Desorption Fourier Transform Ion Cyclotron Resonance Mass Spectrometry", Paper presented at the 34th Annual Conference on Mass Spectrometry and Allied Topics, Cincinnati, OH, June 8–13, 1986.
13. Loo, J.A.; Williams, E.R.; Amster, I.J.; Furlong, J.J.P.; Wang, B.H.; McLafferty, F.W. "Californium-252 Plasma Desorption with Fourier Transform Mass Spectrometry", *Anal. Chem.* **1987,** *59,* 1880–1882.
14. Loo, J.A.; Williams, E.R.; Furlong, J.J.P.; Wang, B.H.; McLafferty, F.W.; Chait, B.T.; Field, F.H. "^{252}Cf Plasma Desorption Fourier Transform Mass Spectrometry of Involatile Compounds", *Int. J. Mass Spectrom. Ion Proc.* **1987,** *78,* 305–313.
15. Viswanadham, S.K.; Hercules, D.M.; Weller, R.R.; Giam, C.S. "^{252}Cf Plasma Desorption Fourier Transform Ion Cyclotron Resonance Mass Spectrometry", *Biomed. Environ. Mass Spectrom.* **1987,** *14,* 43–45.
16. Grotemeyer, J.; Boesl, U.; Walter, K.; Schlag, E.W. "A General Soft Ionization Method for Mass Spectrometry: Resonance-enhanced Multi-photon Ionization of Biomolecules", *Org. Mass Spectrom.* **1986,** *21,* 645–653.
17. Pallix, J.B.; Schuhle, U.; Becker, C.H.; Heustis, D.L. "Advantages of Single-Photon Ionization over Multiphoton Ionization for Mass Spectrometric Surface Analysis of Bulk Organic Polymers", *Anal. Chem.* **1989,** *61,* 805–811.
18. Hsu, A.T.; Marshall, A.G. "Identification of Dyes in Solid Poly(methyl methacrylate) by Means of Laser Desorption Fourier Transform Ion Cyclotron Resonance Mass Spectrometry", *Anal. Chem.* **1988,** *60,* 932–937.
19. Land, D.P.; Pettiette-Hall, C.L.; McIver, R.T., Jr.; Hemminger, J.C. "Detection of Reaction Intermediates in the Conversion of Cyclohexane to Benzene on Pt (111)", *J. Am. Chem. Soc.* **1986,** *111,* 5970–5972.
20. Land, D.P.; Tai, T.-L.; Lindquist, J.M.; Hemminger, J.C.; McIver, R.T., Jr. "Characterization of Multilayer Thin Films by Laser-Induced Thermal Desorption Mass Spectrometry", *Anal. Chem.* **1987,** *59,* 2924–2927.
21. Amster, I.J.; Land, D.P.; Hemminger, J.C.; McIver, R.T., Jr. "Chemical Ionization of Laser-Desorbed Neutrals in a Fourier Transform Mass Spectrometer", *Anal. Chem.* **1989,** *61,* 184–186.

22. Russell, D.H., Ed. "Gas-Phase Inorganic Chemistry", Plenum: New York, 1989.
23. Forbes, R.A.; Tews, E.C.; Huang, Y.; Freiser, B.S.; Perone, S.P. "Evaluation of Laser Desorbed Transition-Metal Ions as Analytical Chemical Ionization Reagents by Pattern Recognition", *Anal. Chem.* **1987,** *59,* 1937–1944.
24. Henry, K.D.; Williams, E.R.; Wang, B.H.; McLafferty, F.W.; Shabanowitz, J.; Hunt, D.F. "Fourier-Transformn Mass Spectrometry of Large Molecules by Electrospray Ionization", *Proc. Natl. Acad. Sci. USA* **1989,** *86,* 9075–9078.
25. Henry, K.D.; McLafferty, F.W. "Electrospray Ionization with Fourier-Transform Mass Spectrometry. Charge State Assignment from Resolved Isotopic Peaks", *Org. Mass Spectrom.* **1990,** *25,* 490–492.
26. Freiser, B.S. "Investigations of Reactions of Metal Ions and Their Clusters in the Gas Phase by Laser-Ionization Fourier-Transform Mass Spectrometry", *Talanta* **1985,** *32,* 697–708.
27. McLafferty, F.W.; Amster, I.J. "Tandem Fourier-Transform Mass Spectrometry", *Int. J. Mass Spectrom. Ion Proc.* **1986,** *72,* 85–91.
28. Cody, R.B.; Burnier, R.C.; Cassady, C.J.; Freiser, B.S. "Consecutive Collision-Induced Dissociations in Fourier Transform Mass Spectrometry", *Anal. Chem.* **1982,** *54,* 2225–2228.
29. Gord, J.R.; Freiser, B.S. "Separation of Experiments in Time and Space Using Dual-Cell Fourier-Transform Ion Cyclotron Resonance Mass Spectrometry", *Anal. Chim. Acta* **1989,** *225,* 11–24.
30. Kerley, E.L.; Russell, D.H. "Mass and Energy Selective Ion Partitioning in a Two-Section Fourier Transform Ion Cyclotron Resonance Spectrometer Cell", *Anal. Chem.* **1989,** *61,* 53–57.
31. Hanson, C.D.; Kerley, E.L.; Russell, D.H. "High-Resolution Ion Partitioning Technique by Phase-Specific Ion Excitation for Fourier Transform Ion Cyclotron Resonance", *Anal. Chem.* **1989,** *61,* 83–85.
32. Farrell, J.T.; Lin, P.; Kenttamaa, H.I. "A Simple Method for Ion Isolation in Fourier Transform Ion Cyclotron Resonance Mass Spectrometry: Combined Notch Excitation and Selective Ion Partitioning in a Dual Cell", *Anal. Chim. Acta,* in press.
33. Cody, R.B. "Accurate Mass Measurements on Daughter Ions from Collisional Activation in Fourier Transform Mass Spectrometry", *Anal. Chem.* **1988,** *60,* 917–923.
34. Wise, M.B. "Ultra-High-Resolution Daughter Ion Tandem Mass Spectra Using a Differentially Pumped Dual Cell Fourier Transform Mass Spectrometer", *Anal. Chem.* **1987,** *59,* 2289–2293.
35. Dunbar, R.C. In "Gas Phase Ion Chemistry", Bowers, M.T. Ed.; Academic Press: New York, 1984; Vol. 3, Chapter 20.
36. Nuwaysir, L.M.; Wilkins, C.L. "Photodissociation of Laser-Desorbed Ions as a Structure Determination Tool", *Anal. Chem.* **1989,** *61,* 589–694.
37. Bowers, W.D.; Delbert, S.-S.; McIver, R.T., Jr. "Consecutive Laser-Induced Photodissociation as a Probe of Ion Structure", *Anal. Chem.* **1986,** *58,* 969–972.

38. Asamoto, B.; Dunbar, R.C. "Photodissociation Spectroscopy of Several $C_5H_6^+$ Isomeric Ions", *Int. J. Mass Spectrom. Ion Proc.* **1988,** *86,* 387–400.
39. Marshall, A.G.; Verdun, F.R. "Fourier Transforms in NMR, Optical, and Mass Spectrometry"; Elsevier: Amsterdam, 1990.
40. Comisarow, M.B. "Signal Modeling for Ion Cyclotron Resonance", *J. Chem. Phys.* **1978,** *69,* 4097–4104.
41. Dunbar, R.C. "The Effect of Ion Position on ICR Signal Strength", *Int. J. Mass Spectrom. Ion Proc.* **1984,** *56,* 1–9.
42. McIver, R.T., Jr.; Baykut, G.; Hunter, R.L. "Theory of Impulse Excitation for Fourier Transform Mass Spectrometry", *Int. J. Mass Spectrom. Ion Proc.* **1989,** *89,* 343–358.
43. McIver, R.T., Jr.; Hunter, R.L.; Baykut, G. "Impulse Excitation for Fourier-Transform Mass Spectrometry", *Anal. Chem.* **1989,** *61,* 489–491.
44. Comisarow, M.B.; Marshall, A.G. "Frequency-Sweep Fourier Transform Ion Cyclotron Resonance Spectroscopy", *Chem. Phys. Lett.* **1974,** *26,* 489–490.
45. Kofel, P.; Allemann, M.; Kellerhals, H.P.; Wanczek, K.P. "Coupling of Axial and Radial Motions in ICR Cells During Excitation", *Int. J. Mass Spectrom. Ion Proc.* **1986,** *74,* 1–12.
46. Marshall, A.G.; Wang, T.-C.; Ricca, T.L. "Tailored Excitation for Fourier Transform Ion Cyclotron Resonance Mass Spectrometry", *J. Am. Chem. Soc.* **1985,** *107,* 7893–7897.
47. Goodman, S.; Hanna, R. U.S. Patent 4,945,234, 1986.
48. Guan, S. "General Phase Modulation Method for Stored Waveform Inverse Fourier Transform Excitation for Fourier Transform Ion Cyclotron Resonance Mass Spectrometry", *J. Chem. Phys.* **1989,** *91,* 775–777.
49. Lee, J.P.; Comisarow, M.B. "Advantageous Apodization Functions for Absorption-Mode Fourier Transform Spectroscopy", *Appl. Spectrosc.* **1989,** *43,* 599–604.
50. Aarstol, M.; Comisarow, M.B. "Apodization of FT-ICR Spectra", *Int. J. Mass Spectrom. Ion Proc.* **1987,** *76,* 287–297.
51. Brenna, J.T.; Creasy, W.R. "Experimental Evaluation of Apodization Functions for Quantitative Fourier Transform Mass Spectrometry", *Int. J. Mass Spectrom. Ion Proc.* **1989,** *90,* 151–166.
52. de Koning, L.J.; Kort, C.W.F.; Pinske, F.A.; Nibbering, N.M.M. "Segmented Fourier Transform and Its Application to Fourier Transform Ion Cyclotron Resonance (FT-ICR) Mass Spectrometry: Ion Abundances and Mass Measurements," *Int. J. Mass Spectrom. Ion Proc.* **1989,** *95,* 71–92.
53. Mitchell, D.W.; DeLong, S.E., "Initial Relative Ion Abundances and Relaxation Times from Apodized, Segmented FT/ICR Time-Domain Signals", *Int. J. Mass Spectrom. Ion Proc.* **1990,** *96,* 1–16.
54. Williams, C.P.; Marshall, A.G. "Hartley Transform Ion Cyclotron Resonance Mass Spectrometry", *Anal. Chem.* **1990,** *61,* 428–431.
55. McLafferty, F.W.; Stauffer, D.B.; Loh, S.Y.; Williams, E.R. "Hadamard

Transform and No-Peak Enhancement in Measurement of Tandem Fourier Transform Mass Spectra", *Anal. Chem.* **1987,** *59,* 2212–2213.

56. Meier, J.E.; Marshall, A.G. "Bayesian versus Fourier Spectral Analysis of Ion Cyclotron Resonance Time-Domain Signals", *Anal. Chem.* **1990,** *62,* 201–208.
57. Rahbee, A. "Application of Maximum Entropy Spectral Analysis to Fourier Transform Mass Spectrometry", *Chem. Phys. Lett.* **1985,** *117,* 352–358.
58. Pfandler, P.; Bodenhausen, G.; Rapin, J.; Houriet, R.; Gaumann, T. "Two-Dimensional Fourier Transform Ion Cyclotron Resonance Mass Spectrometry", *Chem. Phys. Lett.* **1987,** *138,* 195–199.
59. Hunter, R.L.; Sherman, M.G.; McIver, R.T., Jr. "An Elongated Trapped-Ion Cell for Ion Cyclotron Resonance Mass Spectrometry with a Superconducting Magnet", *Int. J. Mass Spectrom. Ion Phys.* **1983,** *50,* 259–274.
60. Lee, S.H.; Wanczek, K.P.; Hartmann, H. "A New Cylindrical Trapped Ion ICR Cell", *Adv. Mass Spectrom.* **1980,** *88,* 1645–1649.
61. Wang, M.; Marshall, A.G. FACSS XIV Annual Meeting, Detroit, Mich., October 1987; Abstr. 43.
62. Wang, M.; Marshall, A.G. "A Screened Electrostatic Ion Trap for Enhanced Mass Resolution, Mass Accuracy, Reproducibility, and Upper Mass Limit in Fourier Transform Ion Cyclotron Resonance Mass Spectrometry," *Anal. Chem.* **1989,** *61,* 1288–1293.
63. Wang, M.; Marshall, A.G. "Elimination of z-Ejection in Fourier Transform Ion Cyclotron Resonance Mass Spectrometry by Radio Frequency Electric Field Shimming", *Anal. Chem.* **1990,** *62,* 515–520.
64. Hanson, C.D.; Castro, M.E.; Kerley, E.L.; Russell, D.H. "Field-Corrected Ion Cell for Ion Cyclotron Resonance", *Anal. Chem.* **1990,** *62,* 520–526.
65. Sommer, H.; Thomas, H.A.; Hipple, J.A. "The Measurement of e/M by Cyclotron Resonance", *Phys. Rev.* **1951,** *82,* 697–702.
66. Cody, R.B.; Kinsinger, J.A. "Making Use of Information Contained in Folded-Back Peaks to Identify Low Mass Ions in Fourier Transform Mass Spectrometry", *Anal. Chem.* **1986,** *58,* 670–671.
67. Cody, R.B.; Kinsinger, J.A. In *"FTMS, Evolution, Innovation, and Applications"*; Buchanan, M., Ed.; ACS: Washington, 1987.
68. Littlejohn, D.P.; Ghaderi, S. U.S. Patent 4,581,533, 1986.
69. Asamoto, B. "Fourier Transform-Mass Spectrometry for Industrial Problem Solving", *Spectroscopy* **1988,** *3,* 38–46.
70. Kofel, P.; Allemann, M.; Kellerhals, H.P.; Wanczek, K.P. "External Generation of Ions in ICR Spectrometry", *Int J. Mass Spectrom. Ion Proc.* **1985,** *65,* 97–103.
71. Caravatti, P. Spectrospin AG, U.S. Patent 4,924,089, 1990.
72. McIver, R.T., Jr.; Hunter, R.L.; Bowers, W.D. "Coupling a Quadrupole Mass Spectrometer and a Fourier Transform Mass Spectrometer", *Int. J. Mass Spectrom. Ion Proc.* **1985,** *64,* 67.
73. Comisarow, M.B. "Fundamental Aspects and Applications of Fourier", *Anal. Chim. Acta* **1985,** *178,* 1–15.

74. Marshall, A.G.; Comisarow, M.B.; Parisod, G. "Relaxation and Spectral Line Shape in Fourier Transform Ion Cyclotron Resonance Spectroscopy", *J. Chem. Phys.* **1979,** *71,* 4434–4444.
75. Bamberg, M.; Allemann, M.; Wanczek, K.P. *Int. J. Mass Spectrom. Ion Proc. 95,* in press; or Wanczek, K.P. "ICR Spectrometry—A Review of New Developments in Theory, Instrumentation, and Applications. I. 1983–1986", *Int. J. Mass Spectrom. Ion Proc.,* **1989,** *95,* 1–38.
76. Allemann, M.; Grossmann, P.; Kellerhals, H.P. "Ultrahigh Resolution Mass Spectrometry using the CMS-47", *Information ICR (Spectrospin application note)* **1986,** *V.*
77. Ijames, C.F.; Wilkins, C.L. "First Demonstration of High Resolution Laser Desorption Mass Spectrometry of High Mass Organic Ions", *J. Am. Chem. Soc.* **1988,** *110,* 2687–2688.
78. Lebrilla, C.B.; Wang, D.T.S.; Hunter, R.L.; McIver, R.T., Jr. "Detection of Mass 31830 Ions with an External Ion Source Fourier Transform Mass Spectrometer", *Anal. Chem.* **1990,** *62,* 878–880.
79. Nicolet FTMS-2000 mass spectrometer with a 3T magnet.
80. Schuch, D.; Chung, K.-M.; Hartmann, H. "Effect of Magnetic Field Inhomogeneity on Exact Mass Determination in ICR Spectrometry", *Int. J. Mass Spectrom. Ion Proc.* **1984,** *56,* 109–121.
81. White, R.L.; Onyiriuka, E.C.; Wilkins, C.L. "Exact Mass Measurement in the Absence of Calibrant by Fourier Transform Mass Spectrometry", *Anal. Chem.* **1983,** *55,* 339–343.
82. Ledford, E.B., Jr.; Rempel, D.L.; Gross, M.L. "Space Charge Effects in Fourier Transform Mass Spectrometry. Mass Calibration", *Anal. Chem.* **1984,** *56,* 2744–2748.
83. Jeffries, J.B.; Barlow, S.E.; Dunn, G.H. "Theory of Space-Charge Shift of Ion Cyclotron Resonance Frequencies", *Int. J. Mass Spectrom. Ion Proc.* **1983,** *54,* 169–181.
84. Laude, D.A., Jr.; Beu, S.C. "Suspended Trapping Pulse Sequence for Simplified Mass Calibration in Fourier Transform Mass Spectrometry," *Anal. Chem.* **1989,** *61,* 2422–2427.
85. Hofstadler, S.A.; Laude, D.A., Jr. "Fourier Transform Mass Spectrometric Detection of Suspended Trapping Measurements with a Variable Length External Ion Reservoir", *Int. J. Mass Spectrom. Ion Proc.* **1990,** *97,* 151–164.
86. Hogan, J.D.; Laude, D.A., Jr. "Suspended Trapping Procedure for Alleviation of Space Charge Effects in Gas Chromatography/Fourier Transform Mass Spectrometry", *Anal. Chem.* **1990,** *62,* 530–535.
87. Smith, M.J.C. Private communication, February 1, 1990.
88. Hays, J.D.; Dunbar, R.C. "Array-Processor-Based Fourier-Transform Ion Cyclotron Resonance Mass Spectrometer", *Rev. Sci. Instrum.* **1984,** *55,* 1116–1119.
89. W.D. Reents, Jr. "Impurities in Boron Trichloride and Boron Trifluoride Determined by Fourier Transform Mass Spectrometry", *Anal. Chem.* **1986,** *58,* 2797–2800.
90. Wang, T-C.L.; Ricca, T.L.; Marshall, A.G. "Extension of Dynamic Range

in Fourier Transform Ion Cyclotron Resonance Mass Spectrometry via Stored Waveform Inverse Fourier Transform Excitation", *Anal. Chem.* **1986,** *58,* 2935–2938.

91. Grosshans, P.B.; Wang, M.; Marshall, A.G. In 36th ASMS Conference on Mass Spectrometry and Allied Topics," 1988; pp 592–593.
92. So, H.Y.; Wilkins, C.L. "First Observation of Carbon Aggregate Ions $>C_{600}$ by Laser Desorption Fourier Transform Mass Spectrometry", *J. Phys. Chem.* **1989,** *93,* 1184–1187.
93. Hunt, D.F.; Shabanowitz, J.; Yates, J.R., III; Zhu, N.-Z; Russell, D.H.; Castro, M. "Tandem Quadrupole Fourier-Transform Mass Spectrometry of Oligopeptides and Small Proteins", *Proc. Natl. Acad. Sci. USA* **1987,** *84,* 620–623.
94. Dunbar, R.C. "Time-Resolved Unimolecular Dissociation of Styrene Ion: Rates and Activation Parameters", *J. Am. Chem. Soc.* **1989,** *111,* 5572; "Kinetic Parameters for the Unimolecular Dissociation of Styrene Ion", *J. Phys. Chem.* **1990,** *94,* 3283.